The dodecahedron web and its instanton homology

P. B. Kronheimer and T. S. Mrowka

November 2026

hexagon:2611.00021v1

Foreword

With the exception of this foreword, the present paper is entirely AI-generated by ChatGPT Astra 6, in response to prompts provided by the human authors. Some earlier input came also from Claude Fable.

In [KM1], an SO(3) instanton homology of webs was defined, and it was conjectured there that the dimension of this instanton homology was equal to the number of Tait colorings of the web if the web was planar. The correctness of this conjecture would lead to a proof of the four-color theorem, independent of the work of Appel and Haken. Since 2013, an important test case has been the dodecahedron web. It has 60 Tait colorings. The dimension of its instanton homology was eventually shown to be bounded below by 60 and bounded above by 64 (with the latter bound being due to David Boozer in unpublished work). The paper here presents a proposed proof that the instanton homology has dimension 64, contradicting the conjecture.

The AI-generated text uses the term "proposed theorem" not because any gaps or weaknesses in the argument are known, but because the paper has not been subject to any human expert review. We use the same language, and for the same reason. In particular, the authors make no claim to have examined the argument in any detail, though its architecture is clear. The authors believe that a human-readable version of the proof, written to high journal-ready standards, could be considerably shorter, and the intention is to produce such a version in due course. The work in its present form is being provided here because timeliness seems valuable.

The argument begins with algebraic steps which reduce the calculation of the dimension to determining whether three mod-2 scalars vanish. Each scalar is a count of instantons on a closed foam equipped with a 1-parameter family of metrics. All three scalars are shown to vanish by demonstrating that the relevant instantons would live in moduli spaces with negative action.

The paper is accompanied by the LaTeX source for this foreworded version, as well as the original source from ChatGPT. The latter is in a folder which includes also ChatGPT's extensive calculations which underlie the algebraic parts of the argument.

Acknowledgements. The work of the first author was supported by NSF grant DMS-2304877. Both authors were supported by Simons Foundation Awards #994330 and #14760-09, *Simons Collaboration on New Structures in Low-Dimensional Topology.*

Abstract

For the planar dodecahedron web D, the octahedral diagram of instanton homology reduces the possible values of $\dim_{\mathbb{F}_2} J^\#(D)$ to 60 and 64. The remaining choice is determined by three coefficients of a secondary map. We give a proposed proof that all three vanish and that the dimension is 64. We express the coefficients as counts of instantons on specified foam cobordisms with one-parameter families of metrics. The index calculation requires these instantons to have negative action. An estimate uniform under neck stretching excludes them when the perturbations are sufficiently small. The construction includes local Floer complexes with zero differential, the marking calculation for excision, and a simultaneous choice of regular perturbations compatible with the families. Exact matrices and the supporting foam calculations are provided separately.

Contents

1 Introduction **3**

2 The octahedral calculation **6**

3 Floer complexes for the local webs **18**

4 Local relations and geometric chain homotopies **25**

5 The secondary operation and its normalization **34**

6 The index calculation for the closed foams **37**

7 Perturbations and the action estimate **44**

8 Assembly of the proposed proof **56**

A Computational specification and reproducibility **57**

1 Introduction

A web is a trivalent graph embedded in $\mathbb{R}^3$, with the local model of three coplanar rays at each vertex. A Tait coloring assigns one of three colors to each edge, with three distinct colors at each vertex. Colors are labelled: two colorings related by a permutation of the colors are counted separately.

The instanton homology $J^\sharp(K)$ associates a finite-dimensional vector space over $\mathbb{F}_2$ to a web K. It is defined in [KM1] using $SO(3)$ orbifold connections. The local isotropy group at an edge acts on the fiber by a nontrivial involution; at a vertex, the isotropy representation is the standard Klein four-group in $SO(3)$. A disjoint Hopf link, placed near infinity and equipped with marking data, removes automorphisms from the configuration space. We use this marked theory throughout.

A foam is a cobordism between webs, with three sheets meeting along seams and with isolated tetrahedral points allowed. It induces a map on $J^\sharp$. Foams may also carry dots on their facets; each dot imposes a degree-one cohomological constraint in the moduli-space count. The elementary relations between these maps make it possible to calculate $J^\sharp$ for many planar webs. In particular, a bigon, triangle or square face can be removed by the relations in [KM1, Section 6].

For planar webs the conjecture of [KM1] is

$$\dim_{\mathbb{F}_2} J^\sharp(K) = \#\{\text{Tait colorings of } K\}.$$

The planar dodecahedron D is the first test case to which none of these three face reductions applies. It has sixty Tait colorings. The deformation constructed in [KM3] gives the lower bound $\dim J^\sharp(D) \geq 60$: its generic rank is the Tait count, and the undeformed dimension is at least this rank [KM3, Theorem 1.2 and Corollary 1.3].

Choose an edge of D and consider the local replacements used in the octahedral diagram of [KM2]. The webs agree outside a disk containing this edge and its two endpoints. We denote this common exterior by E; it is shown in Figure 1. Three of the resulting closed webs, denoted K_0, K_1, L_1, can be reduced by the elementary face relations. Their homology groups and the maps between them can therefore be calculated. The six local pictures, together with the maps in the octahedron, are drawn in Figure 2.

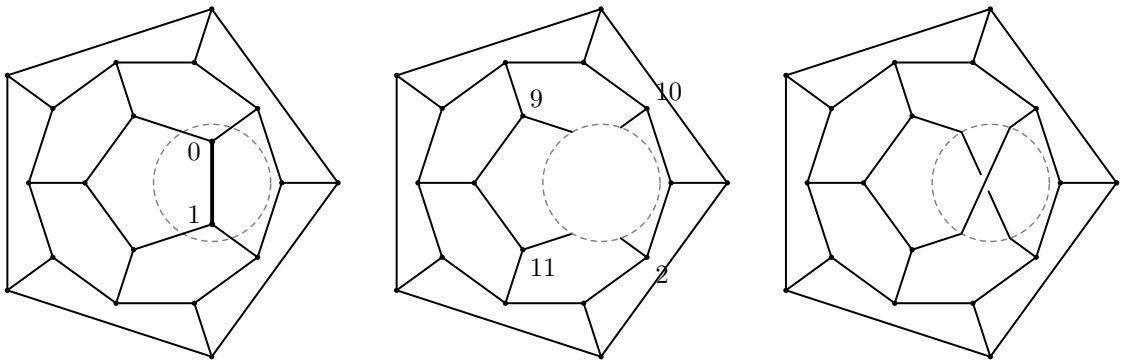


Figure 1: The dodecahedron D, the common exterior E, and K_2, shown with the same planar exterior. Delete the portion inside the dashed circle, including the bold edge 01, to obtain E. Its four ends lead to the labelled vertices $9, 10, 2, 11$, in northwest, northeast, southeast and southwest order. Reinsert two crossing arcs to obtain K_2; the northwest–southeast arc passes underneath. The same four ends are used in Figure 2.

The octahedron does not determine $J^\sharp(D)$ from these calculations alone. There remains a map

h between subquotients of the known groups. It is obtained by lifting through one map in an exact triangle and then applying another; its definition is given in (2.7). The calculation in Section 2 gives

$$\dim J^\sharp(D) = 64 - 2\operatorname{rank} h, \qquad h = \iota \begin{pmatrix} 0 & \alpha & \chi \\ \alpha & 0 & \beta \\ \chi & \beta & 0 \end{pmatrix} \rho, \tag{1.1}$$

where ι is injective and ρ is surjective. Thus the unknown part of the calculation consists of three coefficients in $\mathbb{F}_2$. A nonzero alternating 3×3 matrix over $\mathbb{F}_2$ has rank two, so the two remaining possibilities are 60 and 64. The upper bound here is 64, correcting the value 70 reported in the earlier papers.

Proposed theorem 1.1 (Dodecahedron dimension)**.** *For the planar dodecahedron web D, the three coefficients in* (1.1) *vanish:*

$$\alpha = \beta = \chi = 0, \qquad \dim_{\mathbb{F}_2} J^\sharp(D) = 64.$$

The proposed conclusion would give a counterexample to the planar Tait-coloring conjecture. The word *proposed* records the status of the argument: the complete proof has not received independent expert verification. In particular, the finite calculation leaving 60 or 64 must be distinguished from the local perturbation, excision and index arguments used here to select 64. A proof of the simultaneous choice of geometric data is included as Theorem 7.8, and the argument is assembled in Section 8.

1.1 Outline of the proof

We first explain how the finite calculation is related to the geometry. A foam from the empty web to a web K determines an element of $J^\sharp(K)$, since $J^\sharp(\varnothing) = \mathbb{F}_2$. Reversing the cobordism gives a foam from K to the empty web, and hence a linear functional on $J^\sharp(K)$. Composing these two foams gives a closed foam whose invariant is the value of the functional on the element. This is the pairing used to verify bases and compute matrices in Section 2. The reflection is in the cobordism coordinate; it is not an additional operation on the planar web.

For K_0, K_1, L_1, repeated face reductions supply collections of such foams. Evaluating their pairings gives dimensions $48, 36, 72$ and gives the two map ranks $35, 11$ needed for the octahedron. Dots on edges of the common exterior act on all the groups and commute with all the maps. The resulting module relations, together with the two extensions in the octahedron, constrain h to the form in (1.1). Specified incoming foams and outgoing foams then extract its three coefficients. No identification of $J^\sharp$ with a combinatorial foam homology is used.

To determine these coefficients we need more than relations on homology. The definition of a secondary map involves choosing a primitive for a boundary in a Floer complex. An arbitrary algebraic choice of primitive would give no control over the topology of the four-manifolds on which the relevant moduli spaces are defined. We instead construct the primitive by counting instantons over specified one-parameter families of metrics and perturbations.

The construction begins with the small webs that occur in the local foam relations. In Section 3 we choose perturbations for which their actual Floer complexes have zero differential. A relation between relative homology classes on one of these webs is then an equality between the corresponding relative chains. Section 4 inserts these local relations into the larger cobordisms and constructs the required chain homotopies by stretching necks and applying excision. Combining the homotopies along the sequence of face reductions gives a single primitive for both source cycles that we need.

Section 5 compares this construction with the secondary map h, using the family which proves the exact triangle for the three L-webs.

One point in excision requires particular care. Cutting the composite of the Hopf-excision cobordism and its reverse produces two torus ends. Each has two determinant-one lifts of its flat connection, but the two lifts cannot be quotiented independently. The marking data identify pairs by the simultaneous interchange $(i, j) \mapsto (i + 1, j + 1)$, with indices in $\mathbb{Z}/2$. There are consequently two joint states,

$$\mathcal{T}_\Delta = \mathbb{F}_2\mathfrak{a} \oplus \mathbb{F}_2\mathfrak{b}, \qquad \mathfrak{a} = [00] = [11], \quad \mathfrak{b} = [01] = [10].$$

Both the flat cylinder and the pair of caps select the matching state $\mathfrak{a}$, with multiplicity one. Section 4.3 explains the geometry and marking data behind this assertion.

The final step is an index and action argument. Compose each incoming foam, one-parameter operation and outgoing foam to obtain a capped four-dimensional configuration (X, Σ). Section 6 calculates the part of its index independent of the instanton action:

$$I_{\mathrm{top}} = -\tfrac{3}{2}(\chi(X) + \sigma(X)) + \chi(\Sigma) + \tfrac{1}{2}\nu(\Sigma) - \tfrac{1}{2}\tau(\Sigma) = \tfrac{5}{2}.$$

Here $\nu(\Sigma)$ is the foam self-intersection number and $\tau(\Sigma)$ is the number of tetrahedral points. Including the one family parameter and the dot constraints, a zero-dimensional moduli space would have action $-1/16$ in the three-dot case or $-3/16$ in the two-dot case.

For an unperturbed anti-self-dual connection the action is nonnegative. With holonomy perturbations it need not be, but the energy identity gives a lower bound $\kappa \geq -\delta$, where δ bounds the total error introduced by the perturbations. We must make this error less than $1/16$ for all the cobordisms and families just described, uniformly as their necks become long. Section 7 constructs compatible regular data with this property. Both required negative action values are then excluded, so the three counts vanish.

1.2 Conventions

All vector spaces are over $\mathbb{F}_2$. In Section 2, A, B, C, W denote homology groups. In the later sections the same letters denote geometric Floer complexes for the same webs, with homology HA, HB, HC, HW. We retain the symbols for cobordism maps when passing to homology, specifying the level when it matters. Matrices act on column vectors. Basis subscripts are one-based; arrays and branch indices in the supporting code are zero-based unless otherwise stated.

All action comparisons retain the relative bundle class. The normal number ν is the self-intersection of [KM1, Definition 2.5], not the full relative Euler number of the squared normal bundle. We use no absolute integer grading on general $J^\sharp$. The auxiliary degree labels in the finite data are not such a grading, and the obstruction calculation does not use them.

We take the theory of marked bifold connections, elliptic gauge fixing and ordinary Floer compactification from the cited papers. The additional local perturbations, families and index calculations are developed here. The framed arcs and the specified augmentation of the terminal web are part of the geometric data. An isomorphism between homology groups does not identify their boundary webs: for example, the two composites in the triangle relation have theta and prism boundaries, respectively.

The supporting files contain both the exact linear algebra and the lists of foam moves used to obtain its input. The former can check ranks and identities once the matrices have been supplied; the latter record the geometric calculation of those matrices. Neither replaces a proof of transversality or gluing. Appendix A describes how to reproduce the calculations and the scope of the checks.

2 The octahedral calculation

In this section we calculate the three homology groups in the octahedron which are accessible by face reductions, together with the maps between them. Exactness then expresses $\dim J^\sharp(D)$ in terms of one remaining map h. The edge operators impose further conditions on h, leaving the three coefficients in (1.1).

All the calculations here are on homology, over $\mathbb{F}_2$. In particular, we do not require a Floer complex with zero differential for any of the three large webs K_0, K_1, L_1. When we say that these webs can be reduced, we mean by bigon, triangle and square relations; this has nothing to do with reducibility of a connection.

2.1 The webs and the octahedron

The local pictures are those of [KM2, Figure 1], reproduced with our notation in Figure 2. Outside the displayed disk every web agrees with the exterior E in Figure 1. Thus a local picture specifies an entire closed web, not just a tangle considered in isolation.

For the calculations we also fix vertex labels. Regard D as the planar embedding of the generalized Petersen graph $G(10, 2)$. Its vertices are $0, \dots, 19$, and its unordered edges are

$$\{i, i+1\}, \quad \{i, 10+i\}, \quad \{10+i, 10+(i+2)\}, \qquad i \in \mathbb{Z}/10. \tag{2.1}$$

Only the indices within each set of ten vertices are reduced modulo ten. Choose the edge joining 0 to 1. Delete its two endpoints and the five edges incident to them. The remaining graph has 25 edges and four vertices of valence two, labelled $(9, 10, 2, 11)$ in cyclic order. To regard it as the exterior E, attach a short arc from each of these vertices to the boundary of the deleted disk. The boundary points are northwest, northeast, southeast and southwest, respectively. We use the same four labels for these attaching points. The short arcs are suppressed in the following edge-list notation: adding an edge between two of these labels means joining the corresponding arcs through the disk. The three webs needed for the calculation are

$$\begin{aligned} K_0 &= E + \{9, 10\} + \{2, 11\}, \\ K_1 &= E + \{9, 11\} + \{10, 2\}, \\ L_1 &= E + \{20, 21\} + \{20, 9\} + \{20, 11\} + \{21, 10\} + \{21, 2\}. \end{aligned} \tag{2.2}$$

These are embedded using the planar exterior of D. To specify the embedding for the supporting calculations, take the twelve simple five-cycles of (2.1) as the faces. Orient the lexicographically first cycle positively and orient the others so that adjacent faces traverse their common edge in opposite directions. This records the cyclic order of edges at each vertex, up to the initial choice of orientation. The full lists are in `support/finite/graph_labels.json`.

Put

$$A = J^\sharp(K_0), \quad B = J^\sharp(K_1), \quad C = J^\sharp(L_1), \quad W = J^\sharp(K_2), \quad F = J^\sharp(L_2'), \quad M = J^\sharp(D).$$

Here $D = L_0$. In K_2, the northwest–southeast arc passes below the northeast–southwest arc, as drawn in the figures. The crossing is a projection of two disjoint arcs in $\mathbb{R}^3$, not a vertex of the web. The pertinent exact triangles of [KM2] are

$$\begin{aligned} &A \xrightarrow{a} W \xrightarrow{r} C \xrightarrow{s} A, \qquad W \xrightarrow{b} B \xrightarrow{t} M \xrightarrow{q} W, \\ &A \xrightarrow{\gamma} B \xrightarrow{\lambda} F \xrightarrow{\kappa} A, \qquad C \xrightarrow{\eta} F \xrightarrow{\zeta} M \xrightarrow{\xi} C. \end{aligned} \tag{2.3}$$

The identities needed below are

$$ba = \gamma, \qquad \kappa\eta = s, \qquad \lambda b = \eta r. \tag{2.4}$$

The map γ comes from the saddle cobordism between the two smoothings. The foam defining s has this saddle together with a disk along the internal edge of L_1 that disappears. A dot on an edge outside the disk can be moved through any of these cobordisms. Consequently all the maps commute with the edge operators on E.

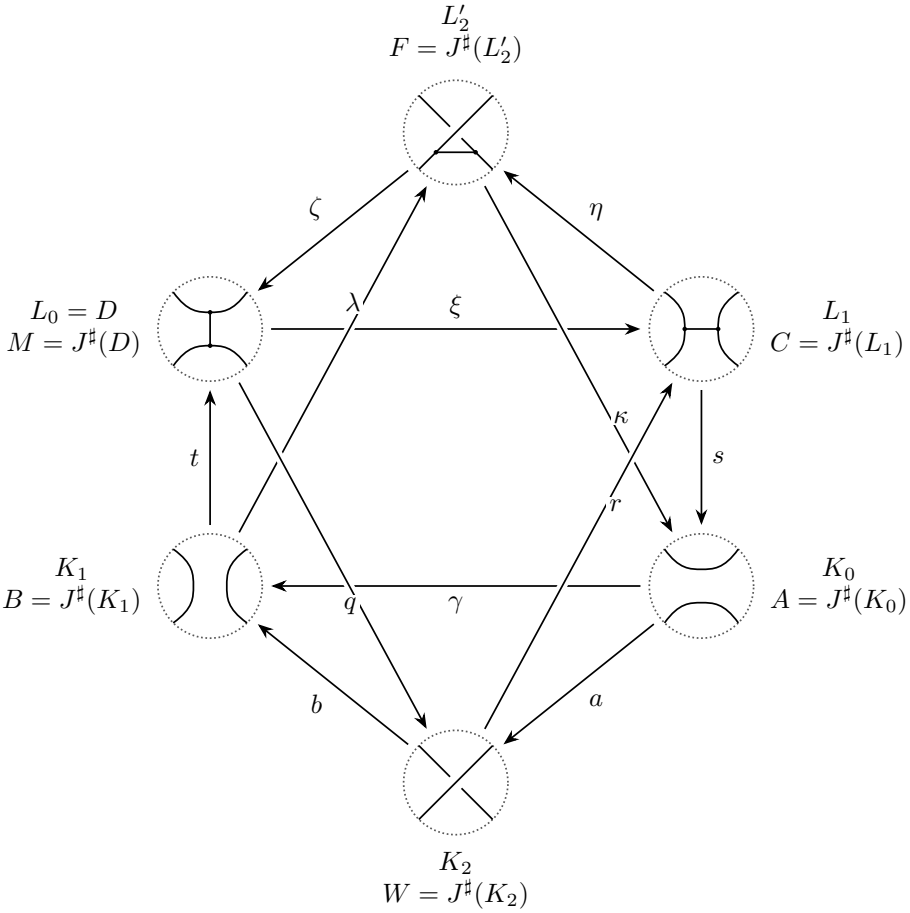


Figure 2: The octahedron of [KM2, Figure 1], with the local webs and the homology groups used here shown together. Each dotted circle is filled into the common exterior E of Figure 1, without rotating the four ends. The four exact triangles are those in (2.3); the other faces express composition identities. The crossing in both K_2 and L_2' has its northwest–southeast strand underneath. Intersections of arrows are not vertices.

We collect these commuting edge operators into an algebra R. For each of the 25 full edges of E, take one generator, represented geometrically by a dot on that edge in the product cobordism. The algebra is commutative. At a trivalent exterior vertex, with incident variables x, y, z, impose

$$x + y + z = 0, \qquad xy + xz + yz = 0, \qquad xyz = 0. \tag{2.5}$$

At a port the third variable means the sum of the two full-edge variables incident to that vertex. Impose the quadratic and cubic relations there as well. Each edge variable satisfies $x^3 = 0$. These

are the actual edge relations of [KM1]; the algebra is not replaced by its image in $\mathrm{End}(A \oplus B \oplus C)$. Eliminating the 14 independent linear relations leaves eleven generators. A presentation uses their 55 commutators, the 18 quadratic and 18 cubic vertex relations, and their eleven cubes. The cube of any dependent edge follows from (2.5): if $z = x + y$, then $x^2 + xy + y^2 = xy(x + y) = 0$ implies $x^3 = y^3 = z^3 = 0$.

We now isolate the information about the two unknown groups W, F which is needed to recover M. Set

$$V = \ker s, \quad U = \operatorname{coker} \gamma, \quad P = \operatorname{coker} s, \quad Z = \ker \gamma, \quad Q = Z/\operatorname{im} s. \tag{2.6}$$

If $v \in V = \ker s$, exactness gives a lift $w \in W$ with $r(w) = v$. Apply b and pass to $U = B/\operatorname{im} \gamma$. This defines the secondary map $h : V \to U$ by

$$h(v) = [b(w)]. \tag{2.7}$$

Two choices differ by $a(x)$, and $ba(x) = \gamma(x)$, so this is well-defined. The same observation with each exterior dot proves that h is R-linear.

Proposition 2.1. *For the octahedron* (2.3)*,*

$$\dim M = \dim A + \dim B + \dim C - 2 \operatorname{rank} s - 2 \operatorname{rank} \gamma - 2 \operatorname{rank} h.$$

Proof. Exactness gives $\dim W = \dim A + \dim C - 2 \operatorname{rank} s$. The subspace $\operatorname{im} \gamma$ lies in $\operatorname{im} b$ by $ba = \gamma$, and the image of $\operatorname{im} b$ in $B/\operatorname{im} \gamma$ is precisely $\operatorname{im} h$. Thus $\operatorname{rank} b = \operatorname{rank} \gamma + \operatorname{rank} h$. Apply the dimension identity for the second triangle in (2.3). □

2.2 Bases defined by foams

We next explain the bases used to calculate the maps s and γ. A foam I from the empty web to K gives a class $J^\sharp(I)(1) \in J^\sharp(K)$. The elementary face relations provide such classes by reversing a sequence of reductions of K to small webs. For a bigon there are two creation foams, distinguished by a dot; for a square the two resolutions give two collections of classes. A triangle has a single reduction. Repeating the process for K_0, K_1, L_1 ends at theta webs.

There is also a direct way to check that the resulting classes form bases. Reflect a creation foam I in the cobordism coordinate to obtain $\overline{I}$, now a cobordism from K to the empty web. It defines a functional $J^\sharp(K) \to \mathbb{F}_2$. Joining I_i to $\overline{I}_j$ produces a closed dotted foam, whose invariant is the pairing of the two classes. We will calculate these pairings using the foam relations of [KM1]. Thus the matrix input comes from maps in $J^\sharp$ itself; no comparison with a combinatorial foam theory is assumed.

Here are the ordering conventions which specify the classes uniquely. Give every graph the lexicographic ordering of its unordered edge list. Find a cycle by depth-first search, starting at the least vertex and taking incident edges in this order. Search first for a bigon, then a triangle, then a square. Use the standard creation foams for the inverse reductions. A new vertex produced by triangle collapse receives the least unused label greater than every current label. For a square with cyclically ordered exterior legs $0, 1, 2, 3$, the two branches are ordered $(01, 23)$ and $(03, 12)$. The search is repeated in each branch, in depth-first order. For these three webs every selected cycle is facial in the inherited rotation system. This is a finite check, recorded with the full reduction trees.

A bigon contributes the undotted creation and the creation with a dot on its first cycle edge. At a terminal theta web use the six foams

$$x^i y^j \theta_-, \qquad 0 \le i \le 2, \quad 0 \le j \le 1,$$

where θ_- is the standard foam from the empty web to the theta web, and x, y place dots on its first two facets at the outgoing edges. These are the "half-foams" used below: each has one empty end, and becomes a closed foam after composition with a reflected half-foam. Several examples are drawn in Section 2.5. Exponents and branches are ordered lexicographically; the complete basis records give the edge and stage of every dot. Write the resulting classes as $A_1, \dots, A_{48}$, $B_1, \dots, B_{36}$ and $C_1, \dots, C_{72}$. The dimension formulas for bigons, triangles and squares in [KM1, Propositions 6.5–6.8] give the same dimensions. Ignoring dots, the branch sizes are

$$A : (24, 6, 6, 12), \qquad B : (12, 12, 12), \qquad C : (12, 12, 12, 12, 12, 12). \tag{2.8}$$

The assertion that these particular half-foams are bases can also be checked by their nonsingular Gram matrices, as follows.

For $X = A, B, C$, let I_i^X denote the creation foam representing the ith class in the corresponding group. Its reflection $\overline{I}_i^X$ has the opposite direction. The pairing matrix and the matrices obtained by inserting s or γ between two such foams are

$$G_X(j,i) = J^\sharp(\overline{I}_j^X I_i^X),$$
$$P_s(j,i) = J^\sharp(\overline{I}_j^A s I_i^C), \qquad P_\gamma(j,i) = J^\sharp(\overline{I}_j^B \gamma I_i^A).$$

We compose from right to left in these formulas. For example, $P_s(j,i)$ is obtained by creating C_i, applying the foam for s, and closing with the reflection of the foam for A_j. The ordinary product Hopf marking stays outside all these moves. A *movie* describes the resulting foam by its successive three-dimensional slices. There are 97 movies after the dots have been forgotten. Different dot placements give the remaining matrix entries without introducing further underlying foams.

The closed foams can be evaluated by removing pairs of tetrahedral points and then applying neck-cutting. The following form of neck-cutting is convenient for this calculation. Suppose a facet closes to an embedded disk Δ, with boundary traversing one seam circle once and with two distinct other incident facets. Put d dots on Δ, and let $F_{a,b}$ be the foam obtained by deleting Δ and its seam, capping the two other facets by parallel copies of Δ, and putting a, b dots on the new caps. Embedded neck-cutting and the theta evaluation give

$$J^\sharp(F) = \sum_{u,v=0}^{2} \Theta(d,u,v) J^\sharp(F_{2-u,2-v}), \tag{2.9}$$

where $\Theta(d,u,v) = 1$ exactly when (d,u,v) is a permutation of $(0,1,2)$. Indeed, two small disjoint push-offs of Δ supply the framed surgery disks in the adjacent sheets. Neck-cutting separates a standard theta foam from $F_{2-u,2-v}$. This proves (2.9) by [KM1, Propositions 5.6 and 6.1]. No compression disk inferred solely from an abstract surface is used.

The supporting record specifies the facets of each movie after separating them along the seams, their Euler characteristics, the order in which their boundaries traverse the seams, and the locations of the dots throughout the reductions. A nonbipartite seam graph gives zero by [KM1, Corollary 8.5], with dots covered by the dotted form of Proposition 8.2, or by dot-to-handle replacement. Otherwise use the embedded cancellation of two tetrahedral points along a seam, [KM1, Proposition 6.7]. Its local boundary is the triangular prism of Figure 11. Follow the three seam-leg pairings and the bands on the opposite corners. After cancellation the certificate checks trivial sheet monodromy and three distinct facets at every seam circle. A connected facet with Euler characteristic one and one boundary component is then an embedded disk to which (2.9) applies. Repetition leaves spheres in $\mathbb{R}^3$, evaluated by [KM1, Proposition 5.3]. Dots are retained on tracked facets at every step.

Family	Movies	Nonbipartite	Reduced to spheres
$\overline{I}_j^A I_i^A$	16	6	10
$\overline{I}_j^B I_i^B$	9	2	7
$\overline{I}_j^C I_i^C$	36	6	30
$\overline{I}_j^A s I_i^C$	24	7	17
$\overline{I}_j^B \gamma I_i^A$	12	9	3
Total	97	30	67

The full list of movies and local replacements is supplied with the draft. These geometric calculations are distinct from the subsequent linear algebra: checking a matrix rank does not establish that its entries are the invariants of the specified embedded foams. The evaluations use the listed relations for $J^\sharp$ and do not assume a general equality between $J^\flat$ and $J^\sharp$.

Proposition 2.2 (Finite pairing calculation)**.** *The specified half-foams have nonsingular Gram matrices of ranks* $48, 36, 72$*. In these bases, the capped evaluations and the exterior dot evaluations give the matrices supplied with this draft, with*

$$\dim(A, B, C) = (48, 36, 72), \qquad \operatorname{rank} s = 35, \qquad \operatorname{rank} \gamma = 11. \tag{2.10}$$

Computational proof and its scope. Construct the 97 movies by stacking the specified reduction half-foams and, when appropriate, the saddle or unzip. The certificate applies the preceding embedded moves, and evaluates their decorations by (2.9) and the sphere rule. Nonsingularity of G_X, together with the independently known dimensions, proves basis completeness. The matrices of the actual maps are consequently

$$s = G_A^{-1} P_s, \qquad \gamma = G_B^{-1} P_\gamma.$$

Adding a dot at an exterior edge computes its action by the same method. The full binary matrices and the move-by-move certificate are supporting data. The independently written checker accompanying this draft verifies (2.10), the vertex relations and all subquotient and intertwining identities from these matrices. It does not constitute a second implementation of the geometric movie evaluator. □

It follows already that $\dim W = 50$ and

$$\dim J^\sharp(D) = 64 - 2 \operatorname{rank} h. \tag{2.11}$$

The dimensions of (P, Z, Q, U, V) are $(13, 37, 2, 25, 37)$.

2.3 The two extension constraints

Commuting with the edge operators is not the only condition on h. It must occur in the actual octahedron, in which the unknown groups W and F are extensions of known R-modules. We spell out the conditions for these extensions to exist. This turns the remaining restriction on h into a linear calculation, without trying to construct W or F geometrically.

The exact sequences

$$0 \longrightarrow Q \longrightarrow P \xrightarrow{\tilde{\gamma}} B \longrightarrow U \longrightarrow 0, \tag{2.12}$$

$$0 \longrightarrow V \longrightarrow C \xrightarrow{s_Z} Z \longrightarrow Q \longrightarrow 0 \tag{2.13}$$

define classes $e \in \mathrm{Ext}^2_R(U,Q)$ and $f \in \mathrm{Ext}^2_R(Q,V)$. The actual octahedron implies $h^*e = 0$ and $h_*f = 0$. The following equations express these two conditions directly in terms of the edge-operator matrices.

Choose vector-space splittings of the short exact sequences furnished by (2.3). For $0 \to P \to W \to V \to 0$, an exterior generator acts by

$$\begin{pmatrix} P_e & \omega_e \\ 0 & V_e \end{pmatrix}, \qquad b = (\bar{\gamma}, f_0).$$

The condition that b be R-linear and induce h is

$$B_e f_0 + f_0 V_e = \bar{\gamma}\omega_e, \qquad \pi f_0 = h, \tag{2.14}$$

where $\pi : B \to U$ is the quotient. In addition the upper triangular matrices must obey every relation of R. For $0 \to U \xrightarrow{\lambda} F \xrightarrow{\kappa} Z \to 0$, write the action and η as

$$\begin{pmatrix} U_e & \omega'_e \\ 0 & Z_e \end{pmatrix}, \qquad \eta = \begin{pmatrix} g_0 \\ s_Z \end{pmatrix}.$$

Then

$$U_e g_0 + g_0 C_e = \omega'_e s_Z, \qquad g_0 i_V = h, \tag{2.15}$$

where $i_V : V \hookrightarrow C$ is the inclusion. The second equality follows from $\eta r = \lambda b$. These equations prove necessity of both extension constraints without asserting that their solutions are realizable by geometric octahedra.

For completeness, the relation equations are linear, including cubic relations. If a word $w = e_1 \cdots e_k$ acts on an extension of Y by X, its upper-right block is

$$\sum_{j=1}^{k} X_{e_1} \cdots X_{e_{j-1}} \omega_{e_j} Y_{e_{j+1}} \cdots Y_{e_k}. \tag{2.16}$$

For a polynomial relation, sum these expressions over its words. There is exactly one unknown block in each term. Thus (2.14) and (2.15), together with (2.16), are finite binary linear systems.

Proposition 2.3 (Computed obstruction space)**.** *There are an injection $\iota : \mathbb{F}_2^3 \to U$ and a surjection $\rho : V \to \mathbb{F}_2^3$, specified in the supporting data, such that the actual map h has the form*

$$h = \iota H \rho, \qquad H = \begin{pmatrix} 0 & \alpha & \chi \\ \alpha & 0 & \beta \\ \chi & \beta & 0 \end{pmatrix}. \tag{2.17}$$

In particular $\operatorname{rank} h$ *is zero or two, and* $\dim J^\sharp(D)$ *is 64 or 60.*

Exact finite verification. First solve all equations $U_e h = h V_e$ on the 925 entries of h; their solution space has dimension 48. Next solve the two full extension systems, retaining all entries as unknowns and eliminating extension variables before the entries of h. No grading or restriction to homogeneous extensions is imposed. For the eleven-generator presentation above the results are

System	Variables	Rank	Constraints on h	Allowed h dimension
(2.14)	7548	6928	922	3
(2.15)	12900	11868	922	3

The two projected three-dimensional subspaces agree. Their union with the three coefficient matrices of $\iota H \rho$ still has dimension three. The checks also give $\operatorname{rank} \iota = \operatorname{rank} \rho = 3$, proving the asserted normal form for every admissible h. The independently written program `support/finite/check_finite.py` constructs these ungraded systems directly from the stored edge matrices. It imports no code from the original evaluator and uses a different set of eleven independent edges. Its outputs include the newly computed bases of both projected spaces.

Finally, a nonzero alternating 3×3 matrix over $\mathbb{F}_2$ has rank two: a nonzero off-diagonal entry gives a nonsingular 2×2 minor, whereas its determinant vanishes. Injectivity of ι and surjectivity of ρ preserve rank. Apply (2.11). □

2.4 Extracting the three coefficients

To use gauge theory to calculate h, we need to express its three coefficients by specified foams at the incoming and outgoing ends. The following choices do this. They fix the coordinates in the normal form (2.17), as well as the dots which will enter the index calculation. Put

$$\begin{aligned} c_1 &= C_{14} + C_{19}, \\ c_2 &= C_4 + C_{40} + C_{65} + C_{68}, \\ c_3 &= C_2 + C_{14} + C_{15} + C_{27} + C_{38} + C_{50} + C_{51} + C_{67}. \end{aligned}$$

These satisfy $s(c_j) = 0$ and $\rho(c_j) = e_j$. Here and below we identify V with its inclusion in C. Reflecting the foam which represents B_i gives a cobordism from K_1 to the empty web. Let $\operatorname{cap}(B_i) : B \to \mathbb{F}_2$ be the resulting functional. Its value on B_j is $G_B(i, j)$, so its matrix is the ith row of the pairing matrix, rather than the ith coordinate covector. Define

$$\begin{aligned} \ell_1 &= \operatorname{cap}(B_2) + \operatorname{cap}(B_7), \\ \ell_2 &= \operatorname{cap}(B_{33}), \\ \ell_3 &= \operatorname{cap}(B_2) + \operatorname{cap}(B_{15}) + \operatorname{cap}(B_{19}) + \operatorname{cap}(B_{26}). \end{aligned}$$

Each ℓ_i annihilates $\operatorname{im} \gamma$ and so descends to U. The supporting matrices verify $\ell_i \iota = e_i^T$; equivalently this can be checked against the three quotient lifts

$$\begin{aligned} x_1 &= B_{11} + B_{18}, \\ x_2 &= B_4 + B_8 + B_9 + B_{16} + B_{17} + B_{21} + B_{28}, \\ x_3 &= B_6 + B_{11}, \end{aligned}$$

for which $[x_j] = \iota(e_j)$ and $\ell_i(x_j) = \delta_{ij}$. Consequently only two sources and two caps are needed:

$$\alpha = \ell_2 h(c_1), \qquad \beta = \ell_2 h(c_3), \qquad \chi = \ell_1 h(c_3). \tag{2.18}$$

Every summand of c_1, c_3 has one dot; the cap B_{33} has two dots, and each of B_2, B_7 has one dot. Thus the three geometric expressions have respectively three, three and two dots. All dot locations are specified by the stage and edge labels in the basis data.

For the last coefficient, it is essential to retain the two caps together. It is their sum $\operatorname{cap}(B_2) + \operatorname{cap}(B_7)$ that annihilates $\operatorname{im} \gamma$; this is not asserted for either summand separately. The source and cap identities, with the caps interpreted as the pairing-matrix rows just described, are checked by the independent linear-algebra calculation.

The classes c_j are represented by the corresponding sums of actual relative foam cycles for any compatible geometric Floer data. The equality $s(c_j) = 0$ in this section means that their images are boundaries, not that the image chain is literally zero. Sections 4 and 5 construct primitives for those boundaries and identify the resulting secondary operation with (2.7); Section 7 supplies their simultaneous analytic control.

2.5 Pictures of the source and cap foams

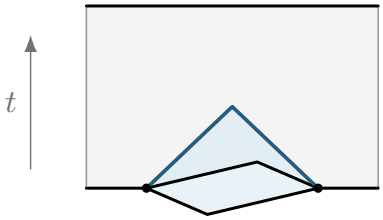
We illustrate some of these basis elements before turning to the gauge theory. The pairs C_{14}, C_{19} and B_2, B_7 each have a common underlying undotted foam; the two members of each pair differ only in the position of one dot. We include B_{33} as well, since the expression for α in (2.18) uses $C_{14} + C_{19}$ at its incoming end and $\mathrm{cap}(B_{33})$ at its outgoing end. The caps of B_2 and B_7 occur in the expression for χ.

It is easiest to draw the foams in the direction of reduction, from the web to the empty web. The creation foam is obtained by reversing this direction. Outside the face being reduced, the edges sweep out product sheets, or "walls". Within that face, sheets close off or join along seams as in Figure 3. There are several such levels in a complete half-foam. In particular, a triangle reduction has a tetrahedral point, where four seams meet. The representatives of C_{14}, C_{19} have two tetrahedral points; those of B_2, B_7 have five, and that of B_{33} has three. A single shaded subset of the original planar web would not, by itself, specify these recorded constructions.

Figures 4–6 give the complete reduction sequences for these examples. In each frame the shaded region is the planar face to which the next elementary foam is applied. Thus it marks the support of a move, rather than an additional sheet lying in the incoming slice. The dashed blue curves are the projections of its seam arcs; at a triangle the fourth seam leaves the plane towards the new vertex. The web is redrawn between frames, with its inherited cyclic orders retained; a different face may be chosen as the unbounded face. Vertex names are those of the reduction record; a name may be reused after its previous vertex has disappeared.

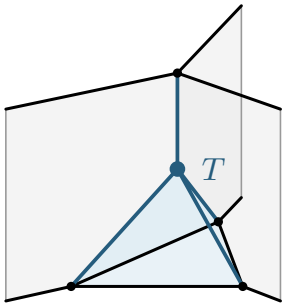
The tuple below a frame gives the vertices of the selected face in cyclic order. At a square, (01)(23) or (03)(12) specifies which successive positions in that tuple are joined by the seam arcs. A colored dot on an edge means a dot on the incident facet, just inside the collar of that slice. It does not mean a marked vertex of the web. Frame numbers start at one; edge numbers in the dot annotations retain the zero-based convention of the supporting records. In the first two movies the marked positions are alternatives: each of the indicated half-foams has one dot. In the movie for B_{33} both positions are used.

Bigon



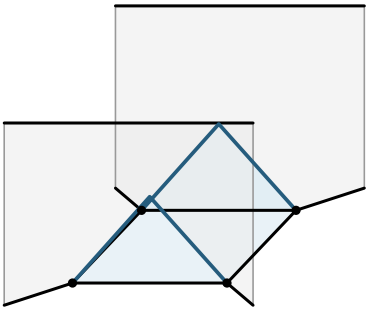
two disks on a common seam
and one sheet continuing upwards

Triangle



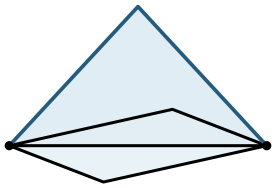
four seams meet at T;
T is a tetrahedral point

Square: one of the two resolutions



two seam arcs; rotate the local picture
through 90° for the other resolution

Terminal theta cap



three disks sharing one seam interval;
the outgoing web is empty

Figure 3: Transparent views of the elementary reduction foams. Time increases upwards. Black curves are boundary webs, blue curves are seams, and the shaded regions are sheets. The faint vertical sides bound the displayed portion of the product sheets. The corners may be rounded. Each local model is extended by the product outside its support; the terminal theta cap has no outgoing web.

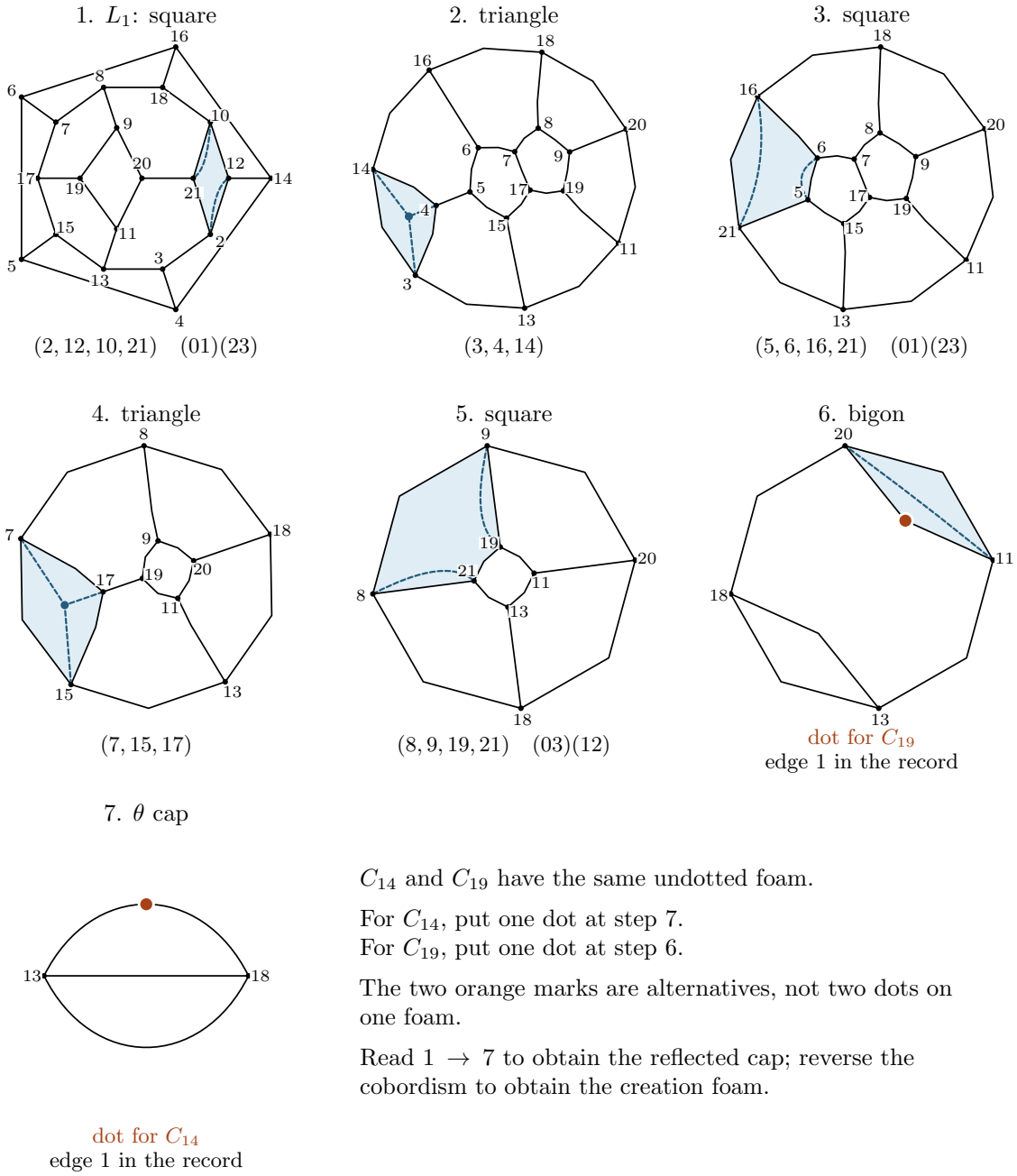


Figure 4: The common reduction movie for C_{14} and C_{19}, beginning with L_1. Read the frames from left to right, then downwards. The creation foams run through these elementary cobordisms in reverse. The choices at the three squares are part of the specification.

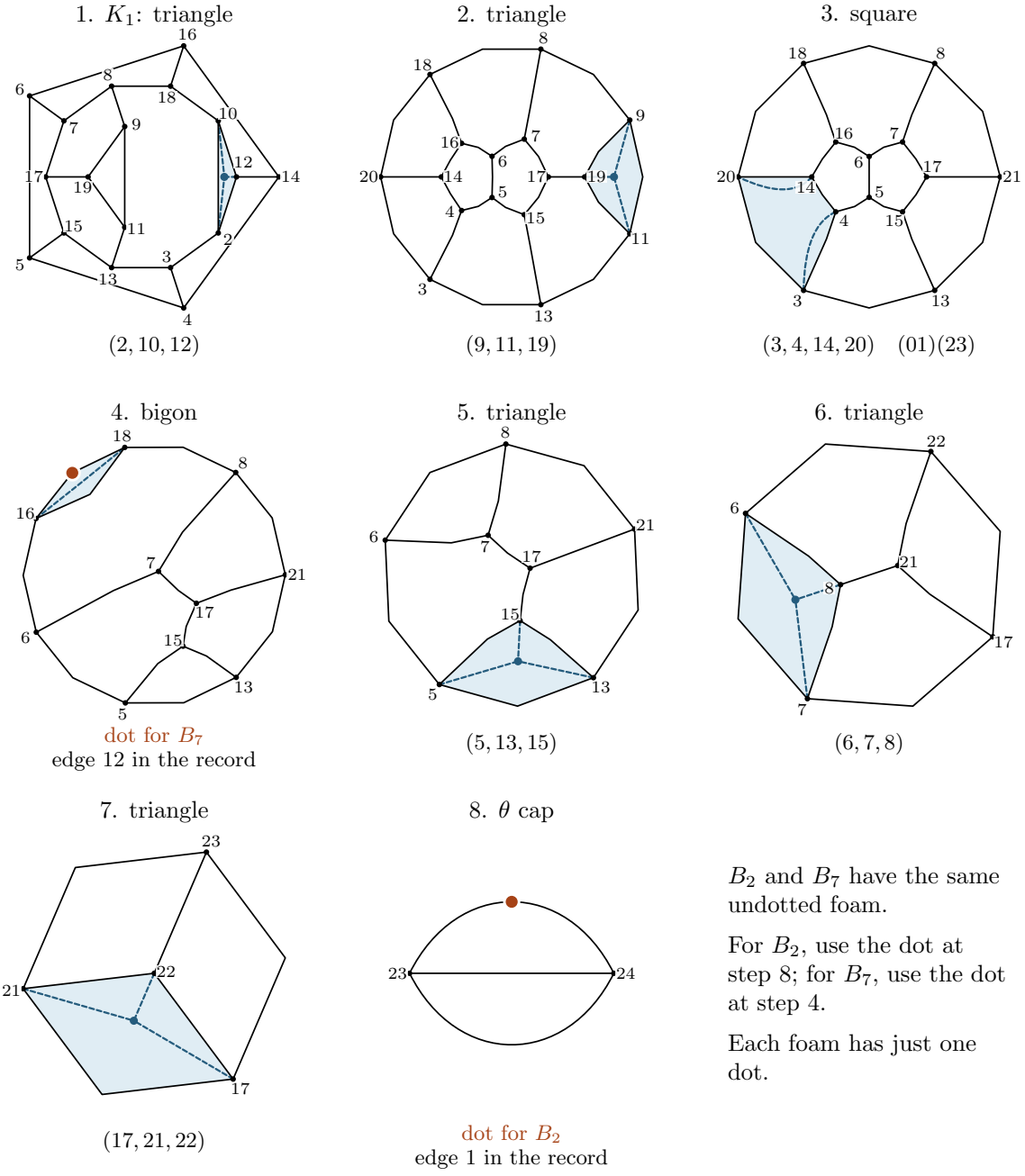


Figure 5: The common reduction movie for B_2 and B_7, beginning with K_1. These are the two dotted caps whose sum defines ℓ_1. The five triangle steps account for the five tetrahedral points of the undotted foam.

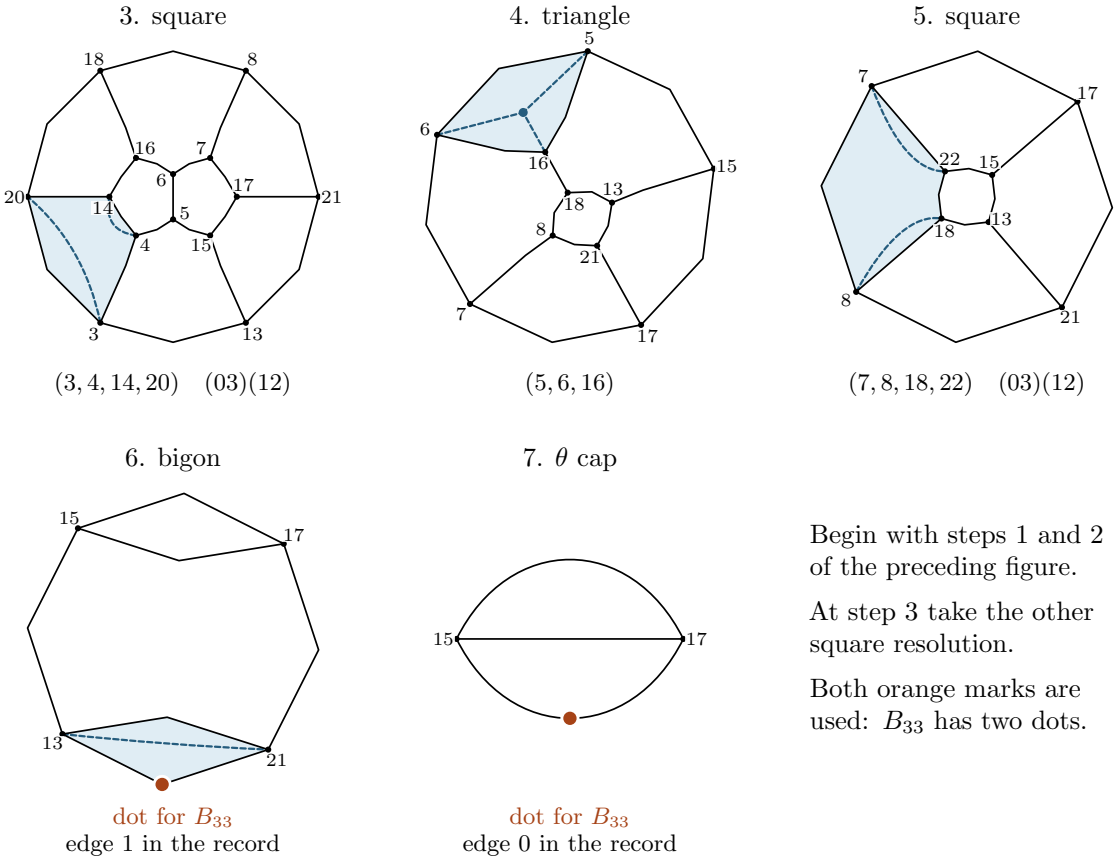


Figure 6: The reduction movie for B_{33} after the first two triangle steps of Figure 5. The different square resolution at step 3 changes the subsequent movie. Both indicated dots are present. This cap represents ℓ_2, which is used in the tests for α and β.

3 Floer complexes for the local webs

The bigon, triangle and square relations in [KM1] are relations between maps on instanton homology. Our argument will also need their chain-level representatives. For example, if two foams with the same boundary define the same homology class, their relative invariants differ by a boundary in the Floer complex of that boundary web. We shall arrange that, for the particular local webs needed here, the differential is zero. The two relative invariants will then be equal as chains.

We call such a choice of Floer complex *perfect*. This means that the complex is defined by nondegenerate critical points and counts of trajectories, with a choice of perturbation for which its differential vanishes. Simply replacing a Floer complex by its homology would not provide the geometric representatives needed later. The task in this section is to construct perfect complexes by choosing the perturbations. Section 4 will explain how to use the resulting local chain relations inside a larger foam cobordism.

Write $\mathcal{F} = SO(3)/V_4$ for the space of ordered triples of mutually orthogonal unoriented lines in $\mathbb{R}^3$. We refer to its points as orthogonal flags. In this section L_n denotes the planar n-sided prism, so that L_4 is the cube. This prism notation is local to this section; it should not be confused with the six webs in the octahedral diagram. Let N be the double-bigon theta web. More explicitly, its vertices are p, q, r, s, t, u, and its edges are

$$pq,\ pr,\ ps,\ qt,\ qu,\ ru,\ ru,\ ts,\ ts.$$

The doubled edges bound the two specified bigons; collapsing both gives the theta web Θ. These webs are drawn in Figure 7; the marking Hopf link is omitted.

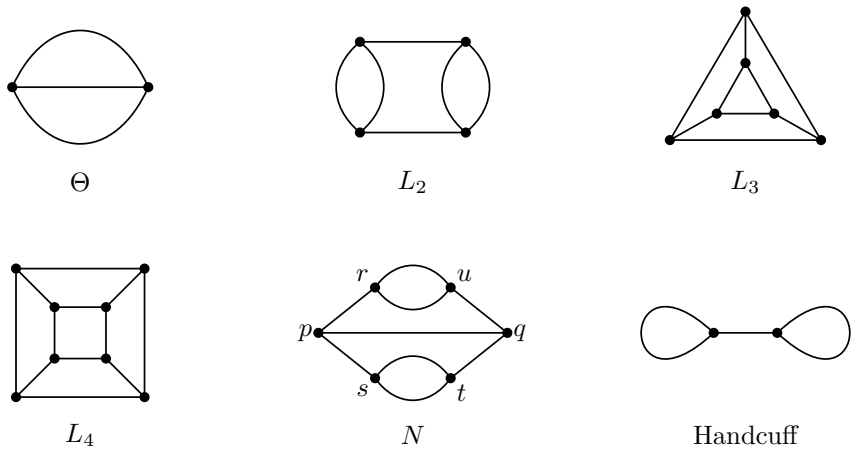


Figure 7: The local boundary webs. Here L_n denotes the n-sided prism, so L_4 is the cube; these labels are distinct from the octahedral labels in Figure 2. Collapsing the two bigons of N gives Θ. All pictures show planar embeddings. The Hopf link used to define $J^\sharp$ is omitted.

Proposition 3.1. *For each of the following planar webs, there are arbitrarily small good holonomy perturbations for which the geometric complex $CF^\sharp(Q)$ has the indicated number of generators and differential zero:*

Q	$\varnothing$	Θ	L_2	L_3	L_4	N
$\dim CF^\sharp(Q)$	1	6	12	6	24	24.

The generators may all be chosen to be flat connections. For each fixed Q, their unperturbed Chern–Simons lifts can be chosen equal. The planar handcuff web has an empty complex for all sufficiently small perturbations.

As in the definition of $J^\sharp$, the Hopf link used for marking is present in every occurrence of $CF^\sharp$. Thus even for the empty web there is a three-dimensional gauge-theory problem: $CF^\sharp(\varnothing)$ is the one-generator complex of the marked Hopf link. This observation matters when the empty-web factor is retained in a cobordism or an excision.

We use the holonomy perturbations and the notion of a good perturbation from [KM1, Section 3.2]. The proof has two parts. First we find small perturbations with exactly the numbers of critical points listed above. We then compare those numbers with known lower bounds for the homology dimensions. Equality forces the differentials to vanish. Most of the flat loci are Morse–Bott; the cube requires a separate analysis at the intersection of three branches.

3.1 Analytic reduction and trace perturbations

The marking allows us to describe the flat connections by holonomy without taking a quotient by overall conjugation. More precisely, [KM1, Lemma 2.10] identifies $\mathcal{R}^\sharp(Q)$ with the representations of the web complement for which every meridian has order two. For a planar web, choose the usual meridians associated to its edges. The holonomy of an edge meridian is a half-turn R_v about an unoriented line v. At a vertex, the three lines are mutually orthogonal. The representation varieties below can therefore be calculated in terms of these lines. The identity

$$\operatorname{tr}(R_v R_w) = 4(v \cdot w)^2 - 1 \tag{3.1}$$

holds for unit representatives. Words in based meridians define the allowed cylinder functions after the usual thickening and integration over a transverse disk. We may include the finitely many functions used here in the defining collection of cylinder functions. This enlargement preserves the analytic estimates and the separation property in the construction of the perturbation space.

Two elementary properties will be useful. The function $(3 - \operatorname{tr} g)/4$ is nonnegative on $SO(3)$ and vanishes at the identity. Also, the differential of trace is zero at the identity and at every half-turn: writing a tangent vector as gX, with X skew symmetric, gives $\operatorname{tr}(gX) = 0$ whenever g is symmetric. Consequently a trace word whose holonomy is an identity or a half-turn has zero differential on the full configuration space. This remains true after thickening, since flat holonomies of the parallel loops are conjugate. Thus the flat critical points constructed below persist exactly, rather than merely up to an unspecified displacement.

Here is the analytic reduction used in the smooth cases. Suppose the entire flat locus M is compact and smooth, and the kernel of the gauge-fixed Chern–Simons Hessian is TM. In a Coulomb slice, its self-adjoint elliptic Hessian is invertible on the normal complement. Compactness of M gives a uniform inverse on finitely many charts. The implicit function theorem therefore solves the normal equation for $\mathrm{CS} + \epsilon f$, and its reduced function on M is

$$\mathrm{CS}\,|_M + \epsilon f|_M + O(\epsilon^2) \tag{3.2}$$

in C^2, uniformly on those charts. If $f|_M$ is Morse, there is precisely one critical point near each of its critical points and none elsewhere near M. If those specified flat points are already critical for the full f, they are the unique resulting critical points.

We also use uniform compactness as the perturbation tends to zero, not merely compactness for each fixed perturbation. For the fixed finite collection of cylinder functions, the perturbed critical equation bounds curvature by a constant tending to zero with the coefficients. Local orbifold gauge fixing on a finite cover, followed by the elliptic estimates for that equation, gives convergence modulo gauge to a flat connection for any sequence of critical points with perturbations tending to zero. The same argument applies in the tame perturbation norm of [KM1, Section 3.2]. Thus a complete

description of the flat locus excludes additional small-perturbation critical points away from its neighborhoods. Strong marking supplies the gauge slices used here. All these statements concern the ordinary three-dimensional critical-point problem; they make no assertion about regularity for a new four-dimensional excision family.

Once finitely many nondegenerate critical points have been obtained, [KM1, Section 3.2] permits a further arbitrarily small good perturbation that vanishes near their neighborhoods. It preserves the critical points and makes the trajectory moduli spaces regular. The absence of other critical points is stable under a sufficiently small such perturbation, by the same compactness argument.

Let h_1, h_2 be the two marked Hopf meridians and put $h_3 = h_1 h_2$. Their flat axes give the reference orthogonal flag. For a vertex with meridians m_1, m_2, m_3, set

$$f_{\mathcal{F}} = \sum_{i,j=1}^{3} \lambda_i \mu_j \frac{\operatorname{tr} \operatorname{Hol}(m_i h_j) + 1}{4}, \qquad \lambda = (0,1,3), \quad \mu = (0,1,4). \tag{3.3}$$

On a flat flag this is $\operatorname{tr}(D_\lambda R^t D_\mu R)$. Its critical equation is $[D_\lambda, R^t D_\mu R] = 0$. Since both diagonal matrices have simple spectra, there are exactly six critical flags. In an ik rotation direction the Hessian is a nonzero multiple of $(\lambda_i - \lambda_k)(\mu_{\sigma(i)} - \mu_{\sigma(k)})$. Every critical point is therefore nondegenerate. At each of these flags every word in (3.3) is an identity or a half-turn, so the full differential vanishes there.

3.2 The smooth local and terminal models

The theta flat space is $\mathcal{F}$. Its Hessian kernel is its tangent space, and (3.3) gives six flat generators by (3.2). Its homology rank is six by [KM1, Proposition 5.7].

For L_3, name the top vertices t_0, t_1, t_2 and the corresponding bottom vertices b_0, b_1, b_2. The top triangle's edge axes are pairwise orthogonal, so write

$$t_0 t_1 = z, \qquad t_1 t_2 = x, \qquad t_2 t_0 = y.$$

The vertical axes are forced to be x, y, z, respectively, and the bottom axes are forced to agree with their corresponding top axes. These assignments satisfy all the bottom vertex relations. They describe the whole representation space, so $\mathcal{R}^\sharp(L_3) = \mathcal{F}$. The description is also valid infinitesimally: each forced axis is a nonzero cross product of two transverse axes, so it is obtained by an invertible local elimination in projective coordinates. No additional infinitesimal variables remain. Equivalently, the orthogonality Jacobian has rank fifteen on the eighteen axis coordinates, with kernel the three simultaneous rotations. Holonomy identifies this kernel with the kernel of the gauge-fixed Chern–Simons Hessian. Thus this is a Morse–Bott flat manifold, and (3.3) gives six flat generators.

The two-sided prism has a different unperturbed flat space. Write its two bigon edge pairs as a, b and u, v, and its other two edges as c, d. The planar meridian presentation gives

$$ab = c = d = uv, \qquad a^2 = b^2 = u^2 = v^2 = c^2 = d^2 = 1.$$

The first vertex determines an orthogonal flag (x, y, z), with $a = R_x$, $b = R_y$, and $c = d = R_z$. The remaining axes are

$$u = R_{\cos\theta\, x + \sin\theta\, y}, \qquad v = R_{-\sin\theta\, x + \cos\theta\, y}, \qquad \theta \in \mathbb{R}/\pi\mathbb{Z}. \tag{3.4}$$

This exhausts the representations. The sign changes of an oriented frame act on θ by reflection, and hence

$$\mathcal{R}^\sharp(L_2) = SO(3) \times_{V_4} \mathbb{RP}^1 = \mathbb{P}(L_x \oplus L_y) \longrightarrow \mathcal{F}, \tag{3.5}$$

where the L_i are the tautological lines. This is a connected smooth four-manifold. The action on the $SO(3)$ factor is free, including at the reflection-fixed fiber points. The elimination leading to (3.4) solves all remaining axes smoothly and over the dual numbers; it leaves exactly one fiber tangent direction. It therefore also proves the Morse–Bott assertion.

The cylinder function

$$q = \frac{3 - \operatorname{tr} \operatorname{Hol}(m_a m_u)}{4}$$

restricts to $\sin^2 \theta$. For any fixed $\delta > 0$, the restriction of $f_{\mathcal{F}} + \delta q$ has exactly twelve Morse critical points, the six coordinate flags with $\theta = 0, \pi/2$. In local flag and fiber coordinates its Hessian is block diagonal, with fiber entry $\pm 2\delta$. All twelve points are full critical points, by the trace observation above. Multiplying this function by a sufficiently small positive number gives precisely twelve nondegenerate flat generators.

Remark 3.2. The literal unperturbed description of L_2 as two flag manifolds in the proof of [KM1, Lemma 5.12] is not used here. Equation (3.4) exhibits the intervening family explicitly: $\operatorname{tr}(R_x R_{\cos\theta x + \sin\theta y}) = 4\cos^2\theta - 1$ varies. Two flag critical manifolds are obtained *after* perturbing by a small multiple of q.

For N, fix the axes at p by $pq = x$, $pr = y$, $ps = z$. The first bigon forces $qu = y$ and the second forces $qt = z$. The two internal ordered axis pairs can be written

$$ru : (\cos\theta\, x + \sin\theta\, z, -\sin\theta\, x + \cos\theta\, z),$$
$$ts : (\cos\phi\, x + \sin\phi\, y, -\sin\phi\, x + \cos\phi\, y).$$

There is no equation coupling θ and ϕ. Thus

$$\mathcal{R}^\sharp(N) = SO(3) \times_{V_4} (\mathbb{RP}^1 \times \mathbb{RP}^1) = \mathbb{P}(L_x \oplus L_z) \times_{\mathcal{F}} \mathbb{P}(L_x \oplus L_y).$$

The same invertible axis eliminations give a smooth five-dimensional Morse–Bott flat manifold. Pairing the first edge of each bigon with pq in the trace formula gives $q_1 = \sin^2\theta$ and $q_2 = \sin^2\phi$. The function $f_{\mathcal{F}} + \delta(q_1 + q_2)$ has exactly $6 \cdot 2 \cdot 2 = 24$ nondegenerate restricted critical points, all full flat critical points. The reduction and compactness arguments give precisely these twenty-four generators.

The empty web has the single nondegenerate flat point of the marked Hopf model. For the planar handcuff, a sphere meeting its bridge once shows that the bridge meridian is null-homotopic in the complement: the meridian contracts on the once-punctured sphere. It cannot have order-two holonomy. There are no flat points, and uniform small-perturbation compactness gives an empty critical set.

3.3 A finite-dimensional lemma for the singular cube model

For the cube, fixing one orthogonal flag leaves three one-dimensional branches of flat connections, meeting at a point. Near that point the normal part of the Chern–Simons function will have the form λxyz, with $\lambda \neq 0$. We first give two elementary lemmas for this singularity. The first removes higher-order terms; the second shows how a small quadratic perturbation of mixed signs leaves only one critical point near the intersection. The estimate in the second lemma is needed to exclude critical points at distances larger than the perturbation scale but still tending to the intersection.

Lemma 3.3. *Let f be a real analytic germ on $\mathbb{R}^3$ whose full differential vanishes on the three coordinate axes, with $f(0) = 0$, zero quadratic part, and cubic part λxyz, where $\lambda \neq 0$. There is an analytic change of variables tangent to the identity taking f to λxyz. The construction is uniform in compact parameter families for which these hypotheses hold and $|\lambda|$ is bounded away from zero.*

Proof. The ideal of analytic germs vanishing on the coordinate axes is $I = (yz, xz, xy)$. This follows by grouping the convergent monomial series according to which two variables occur. Write $f = \lambda xyz + h$. Then h has order at least four, and every component of ∇h belongs to I. With $\mathbf{i} = (yz, xz, xy)^t$, choose analytic $R = O(|(x, y, z)|)$ and $b = O(|(x, y, z)|^2)$ such that $\nabla h = R\mathbf{i}$ and $h = b^t\mathbf{i}$. These choices follow by the same monomial grouping, with convergence on a smaller fixed neighborhood. For $f_t = \lambda xyz + th$, put $M_t = \lambda \mathbf{1} + tR$. Shrinking the neighborhood makes M_t invertible for every $t \in [0, 1]$. The analytic vector field $V_t = -M_t^{-t}b$ has order at least two and satisfies $df_t(V_t) = -h$. Its time-dependent local flow φ_t obeys

$$\frac{d}{dt} f_t(\varphi_t) = h(\varphi_t) + df_t(V_t)(\varphi_t) = 0.$$

Thus $f \circ \varphi_1 = \lambda xyz$. Uniform bounds give the parameter statement. For parameters r the flow fixes r and solves the normal equation fiberwise; no group action on nonflat configurations is needed. □

Lemma 3.4. *Suppose*

$$f_\epsilon(x, y, z) = \lambda xyz + \epsilon q_\epsilon(x, y, z), \quad dq_\epsilon(0) = 0, \quad \operatorname{Hess} q_\epsilon(0) \longrightarrow \operatorname{diag}(a, b, c),$$

where $abc \neq 0$, $\lambda \neq 0$, and the q_ϵ are uniformly C^3 on a fixed neighborhood. If a, b, c have mixed signs, then for all sufficiently small positive ϵ the origin is the only critical point in a fixed neighborhood, and it is nondegenerate. The conclusion is uniform with compact additional parameters and uniform nonzero bounds on the displayed coefficients.

Proof. Let e_ϵ denote the norm of the difference between the Hessian and its diagonal limit. Taylor expansion gives

$$\nabla q_\epsilon = (ax, by, cz) + O(e_\epsilon r + r^2), \qquad r = \max(|x|, |y|, |z|).$$

We claim that every nonzero critical point has $r \leq M\epsilon$ for one fixed M. Suppose, after relabeling, that $|x| = r$, and put $s = \max(|y|, |z|)$. The y, z critical equations give

$$rs \leq C\epsilon(s + e_\epsilon r + r^2).$$

For $r \geq M\epsilon$ with M large enough, absorption yields $s \leq C'\epsilon(e_\epsilon + r)$. On a sufficiently small fixed neighborhood and for small e_ϵ, the x equation then gives

$$\tfrac{1}{2}\epsilon|a|r \leq |\lambda yz| \leq C''\epsilon^2(e_\epsilon + r)^2, \qquad r \leq C'''\epsilon(e_\epsilon + r)^2.$$

Shrinking that neighborhood and then taking ϵ small contradicts $r \geq M\epsilon$, proving the claim.

Rescale $(x, y, z) = \epsilon(u, v, w)$ and divide the gradient equations by ϵ^2. On the resulting fixed compact set, they converge in C^1 to

$$\lambda vw + au = 0, \qquad \lambda uw + bv = 0, \qquad \lambda uv + cw = 0.$$

A nonzero solution must have all three coordinates nonzero, and hence $u^2 = bc/\lambda^2$, $v^2 = ac/\lambda^2$, and $w^2 = ab/\lambda^2$. These equations are impossible for mixed signs. The origin has invertible derivative $\operatorname{diag}(a, b, c)$. Uniform local invertibility excludes additional solutions near it; compactness excludes solutions on the remaining bounded set. The original origin is exactly critical and has nondegenerate Hessian $\epsilon \operatorname{Hess} q_\epsilon(0)$. □

Diagonality in the branch coordinates is essential in this lemma. An arbitrary indefinite quadratic form is not covered. Likewise, rescaling alone would not exclude solutions whose distance is much larger than ϵ; that is the role of the preceding estimate.

3.4 The Chern–Simons function near the cube's flat connections

We now calculate the flat connections on the cube and relate that calculation to the two preceding lemmas. It is necessary to keep track of infinitesimal deformations as well as the set of flat connections: the latter alone would not determine the first nonzero term of the Chern–Simons function.

Number the top square $0,1,2,3$ and the bottom square $4,5,6,7$, with spokes $i(i+4)$. Fix the axes at vertex 0 as $v_{01}=e_1$, $v_{03}=e_2$, $v_{04}=e_3$. Every remaining representation is described by homogeneous coordinates $[A_0:A_1],[B_0:B_1],[C_0:C_1]\in\mathbb{RP}^1$ with

$$\begin{aligned} v_{12}&=(0,A_0,A_1), & v_{15}&=(0,-A_1,A_0),\\ v_{23}&=(B_0,0,B_1), & v_{37}&=(-B_1,0,B_0),\\ v_{45}&=(C_0,C_1,0), & v_{47}&=(-C_1,C_0,0). \end{aligned}$$

The relations at vertices $2,5,7$ are exactly

$$A_1B_1=A_1C_1=B_1C_1=0. \tag{3.6}$$

The axes v_{26},v_{56},v_{67} are forced by cross products; they are nonzero on this solution set, and their vertex-6 equations follow from (3.6). Thus the fixed-frame flat variety is three projective lines meeting at their common origin.

In the affine chart at that origin set $a=A_1/A_0$, $b=B_1/B_0$, $c=C_1/C_0$. The forced remaining vectors are

$$v_{26}=(b,a,-1),\qquad v_{56}=(-c,1,a),\qquad v_{67}=(-1,-c,-b).$$

The three vertex-6 pairings are

$$v_{26}\cdot v_{56}=-bc,\qquad v_{26}\cdot v_{67}=-ac,\qquad v_{56}\cdot v_{67}=-ab. \tag{3.7}$$

Thus the local ideal is exactly (ab,ac,bc). All eliminations used invert nonzero coordinate functions and take nonzero cross products, so this is a scheme-level local calculation, not merely a description of the real zero set. Away from the common point the fixed-frame variety is smooth of dimension one. Restoring the flag gives a six-dimensional Hessian kernel at the common flag and a four-dimensional kernel on the smooth branches.

For clarity we explain why the cubic in the reduced Chern–Simons function is nonzero. The local holonomy correspondence used here also identifies infinitesimal flat deformations, including their second-order obstructions. Indeed parallel transport of a flat connection with coefficients in $\mathbb{R}[t]/(t^3)$ gives a representation over that ring; conversely the representation gives locally constant transition functions and a flat bundle. Gauge equivalence is the corresponding change of trivializations. The finite local isotropy and the fixed marked Hopf factor impose their same relations in both descriptions; the latter is rigid and fixes the local framing. This is the infinitesimal version of [KM1, Lemma 2.10], applied in a gauge slice.

Elliptic Lyapunov–Schmidt reduction at the common flag gives a real analytic reduced potential $g(r,a,b,c)$, where r is a flag chart and a,b,c are the three normal kernel directions. The three smooth flat sheets can simultaneously be straightened onto the three normal coordinate axes: their normal tangent lines are independent, so the sum of their graph parametrizations has invertible differential. All these axes consist of critical points and have the same Chern–Simons value C_0. The normal quadratic part vanishes, and the only possible cubic is

$$g(r,a,b,c)=C_0+\lambda(r)abc+O(|(a,b,c)|^4).$$

Every other cubic monomial has a derivative that is nonzero on some coordinate axis.

If $\lambda(r)$ vanished, the full reduced gradient at that flag would have no quadratic obstruction in the three normal directions. The flag derivatives also have no such term, because the normal Hessian vanishes along the entire flag. Every first-order normal vector would then extend through second order. But the vector $(a, b, c) = (t, t, 0)$ cannot extend to a solution modulo t^3: the coefficient of t^2 in ab is one, independently of all second-order corrections. The infinitesimal holonomy correspondence contradicts the alleged vanishing. Thus $\lambda(r) \neq 0$, uniformly away from zero on finitely many charts of the compact flag. Lemma 3.3 supplies the exact fiberwise form $C_0 + \lambda(r)abc$.

Define the three trace functions

$$q_a = \frac{3 - \operatorname{tr} \mathrm{Hol}(m_{12}m_{03})}{4}, \quad q_b = \frac{3 - \operatorname{tr} \mathrm{Hol}(m_{23}m_{01})}{4}, \quad q_c = \frac{3 - \operatorname{tr} \mathrm{Hol}(m_{45}m_{01})}{4}.$$

On the three flat branches their formulas are respectively $a^2/(1 + a^2)$, $b^2/(1 + b^2)$, and $c^2/(1 + c^2)$. Their normal Hessians at the common flag are diagonal in these branch coordinates. For example q_a is nonnegative on the full configuration space and vanishes at that flag, so its Hessian is positive semidefinite. It vanishes identically along the other two flat branches and the flag; their tangent directions therefore lie in the Hessian kernel, including all mixed entries. Its second derivative along the a-branch is two. The same argument applies to q_b, q_c.

Perturb first by $\epsilon(q_a + q_b - q_c)$. The four Tait flag orbits are exactly critical for this full function. After solving the invertible complement, the limiting normal Hessian at the common flag is $\operatorname{diag}(2, 2, -2)$; the elimination changes it only by terms tending to zero. The flat flag remains exactly critical, so the reduced perturbation has zero normal gradient there. Lemma 3.4 excludes all other nearby normal critical points, uniformly over the flag, and makes the normal Hessian invertible.

At the three outer Tait flags the fiber Hessians are respectively $-2\epsilon, -2\epsilon, 2\epsilon$. On compact portions of the open branches the restricted derivative is nonzero. Ordinary Morse–Bott reduction there, together with the preceding central analysis and uniform small-perturbation compactness, proves that the entire perturbed critical set is precisely four Morse–Bott copies of $\mathcal{F}$. Add $\delta f_{\mathcal{F}}$, with δ chosen sufficiently small *after* ϵ is fixed. Each flag then has its six coordinate critical points, all still flat. The normal inverse may grow as ϵ tends to zero; the stated order of choices accounts for this. There are exactly twenty-four nondegenerate generators. A further good perturbation supported away from them completes the geometric Floer complex.

3.5 Zero differentials, actions and the local chain relations

We have constructed the critical points. To show that the differentials vanish, we use lower bounds for the dimensions of the corresponding homology groups. Each bound comes from a part of the local relations in [KM1] that does not require the chain homotopies we are trying to construct.

For a bigon, the initial bubble-bursting calculation in the proof of [KM1, Proposition 6.5] gives maps with

$$ca = db = 1, \qquad cb = da = 0.$$

They inject two copies of the collapsed web's homology into the expanded web's homology. Starting from the theta rank six, this gives lower bounds twelve for L_2 and twenty-four for N. For L_3, the collapsed-side triangle identity $ca = 1$, proved by theta pairings in [KM1, Proposition 6.6, Figure 10], injects the tetrahedron homology, of rank six by [KM1, Proposition 5.10]. It does not use the triangle-side inverse relation. Finally the initial neck-cutting and bubble-bursting identities in the proof of [KM1, Proposition 6.8] inject the direct sum of the two twelve-dimensional square

resolutions into the cube. They give the lower bound twenty-four before the cube-side inverse relation is established.

Each lower bound equals the number of geometric generators just constructed. For a finite complex over $\mathbb{F}_2$, $\dim H(C,d) = \dim C - 2\operatorname{rank} d$, so $d = 0$ in each case. The marked Hopf unit has the same conclusion immediately. This proves the generator and differential assertions of Proposition 3.1.

Each of the flat spaces above is connected, including the cube's three branches with their common flag. Along a lifted path of flat spatial connections, the four-dimensional curvature in temporal gauge is $dt \wedge \dot{A}$, so its Chern–Weil action is zero. The same calculation applies to loops closing by an allowed marked gauge transformation. The action cover is therefore trivial along the flat locus, giving the common unperturbed lifts asserted in Proposition 3.1. The perturbed critical values generally differ; they are not being identified.

For fixed critical endpoints and Fredholm index, the loop identity $\mathrm{SF} = 8\kappa$ of [KM1, equation (7)] fixes the topological action of all trajectory classes contributing to one differential entry. Thus its zero mod-two count remains zero if that entry is weighted by its topological action. This is an entrywise cancellation statement, not an assertion that individual trajectories are absent. Cancellation among different filling cobordisms requires their own index and dot comparisons.

We can now return to the purpose of this section. A foam filling of a local web defines a relative invariant in its Floer complex. Once one of the perfect complexes above is fixed, such cycles p_j satisfying $\sum_j [p_j] = 0$ satisfy the literal chain equality $\sum_j p_j = 0$. This applies to the local filling relations used in the localization construction, with their actual boundary identifications. In particular the two triangle composites have different local boundaries. Doubling the three-legged star gives Θ, whereas doubling the triangle tangle gives L_3. For the triangle-side relation one must use the L_3 complex and the two fillings in [KM1, Figure 11]. The collapsed-side identity and the rank-six calculation above imply that the expansion–collapse projection on $J^\sharp(L_3)$ is the identity; applying it to the standard filling gives the equality of those two classes, and hence of their relative chains in this complex. This argument supplies the local chain equality. Its transport through a marked exterior, with coherent regular data and the claimed action control, remains the separate localization task.

4 Local relations and geometric chain homotopies

The local relations for foams have a familiar consequence. Suppose several foam cobordisms agree outside a ball, and that the relative invariants of the pieces inside the ball sum to zero. Then the maps induced by the full cobordisms also sum to zero; this is [KM1, Corollary 4.5]. We need a chain-level version of this statement, together with a geometric description of the chain homotopy.

The reason for keeping track of the homotopy is the argument to come. After attaching specified foams at its incoming and outgoing ends, each term will be a count of instantons on a closed foam, with the metric varying in a one-parameter family. The topology of this closed foam enters the index formula. An arbitrary algebraic chain homotopy would not give us the four-manifold and foam needed for that calculation.

We first describe the cobordisms and the families of metrics that will supply these chain homotopies. The marking data, including the framed arcs used to define $J^\sharp$, are part of this description. Proposition 4.2 states that the data can be chosen compatibly for all the families; its analytic proof is deferred to Section 7. We then combine the resulting identities and apply them to the successive local reductions of K_0. This will give a specified chain whose differential is sc, for each of the two source cycles needed in the scalar calculation.

All complexes are over $\mathbb{F}_2$. If $f : E \to F$ is any linear map between complexes, write $\delta f = d_F f + f d_E$. Thus $\delta(fg) = (\delta f)g + f(\delta g)$, and the maps associated to fixed cobordisms are δ-closed. No absolute integer grading on $J^\sharp$ is used in these identities.

4.1 Local fillings, marked arcs and the empty factor

Let $Q \subset S^3$ be the web obtained by intersecting a local foam with the boundary of a four-ball. Suppose that (P_j, Σ_j) is a finite collection of fillings in four-balls, with a fixed identification of their boundaries with (S^3, Q) and a common boundary collar. Removing a small ball disjoint from Σ_j turns a filling into a cobordism from the empty web to Q. Fix the puncture and a framed arc to the basepoint on S^3, common to these fillings and disjoint from every foam. The resulting cobordism defines a chain map

$$p_j : U \longrightarrow D, \qquad U = CF^\sharp(\varnothing), \quad D = CF^\sharp(Q).$$

Here $U = \mathbb{F}_2 u_\varnothing$, with $d_U = 0$, is the geometric Floer complex for the empty web constructed in Section 3. Although it has only one generator, its boundary three-sphere still carries the Hopf link and marking used in the definition of $J^\sharp$. We keep this sphere in all the cobordisms below. The puncture and framed arc are precisely the additional data in [KM1, Definition 3.11]; we do not assert that the construction is independent of the arc.

Suppose the fillings are inserted in cobordisms from a web K to a web K', with a common exterior. Put

$$E = CF^\sharp(K), \quad F = CF^\sharp(K'), \quad S = CF^\sharp(K \sqcup Q),$$

where the split union defining S lies in one connected three-sphere. The letters D, E, F in this local construction are names for complexes; in particular E here is not the four-ended exterior of Section 2. Join the local ball to the incoming boundary by a thin tube in the common exterior, disjoint from the foam and all dots. A regular neighborhood of the incoming collar, tube and ball gives an insertion cobordism. Its map and the map of the remaining exterior have types

$$L_j : E \longrightarrow S, \qquad O : S \longrightarrow F.$$

Write $F_j : E \to F$ for the map of the original cobordism. The local zero-handle and the one-handle given by the joining tube cancel. Thus the insertion cobordism is the boundary connected sum of the cylinder on K and the punctured filling, with their specified arcs. The cylinder on K will be called the *spectator cylinder*: the local replacement does not change its foam. Stretching a neck between the insertion cobordism and the remaining exterior gives a one-parameter family. Its two limits are the original cobordism and the broken composite, so its chain homotopy satisfies

$$\delta R_j = F_j + O L_j. \tag{4.1}$$

If F_j is a product representative, comparison with the strict chain identity requires its product-continuation homotopy as well.

We will also use the excision cobordism that joins two Hopf-marked three-spheres. It transfers K and Q from separate spheres to their split union in one sphere, leaving an empty-web sphere as the other component. This cobordism, which we call the Hopf-excision core, gives chain maps

$$\Psi_{K,Q} : E \otimes D \longrightarrow S \otimes U, \qquad V = \Psi_{K,\varnothing} : E \otimes U \longrightarrow E \otimes U. \tag{4.2}$$

Let V' denote the reverse core map. Both tensor factors in (4.2) represent connected boundary components, including the empty-web components. They cannot be discarded when specifying the four-manifold, markings or bundle sectors.

4.2 Moving the local filling past the excision cobordism

There are two ways to combine the filling p_j with excision. We can first create Q in a separate sphere and then apply $\Psi_{K,Q}$. Alternatively, we can first apply V and then insert the filling into the sphere containing K. Moving the filling from one side of the excision region to the other gives the chain homotopy between these composites. We denote it by N_j; the required identity is

$$\delta N_j = \Psi_{K,Q}(1_E \otimes p_j) + (L_j \otimes 1_U)V, \qquad N_j : E \otimes U \longrightarrow S \otimes U. \tag{4.3}$$

To describe this family, observe that the Hopf surgery in the excision cobordism is disjoint from product regions containing the webs. Choose one such spectator region $\mathbb{R} \times B_Q$ connecting the second incoming sphere to the outgoing sphere containing the split web. Place the compact transition of the punctured filling there, with empty incoming web and outgoing web Q, and with product structure near the lateral boundary. The puncture and framed basepoint arc lie outside this product ball. Translate the transition along the $\mathbb{R}$ coordinate. At one end it occurs before excision, and at the other it occurs after excision. These are exactly the two compositions in (4.3). There is one relative-position parameter. At finite parameter values an isotopy supported in the spectator tube identifies the underlying marked cobordism; the family can be viewed as a family of pulled back metrics and perturbations on that fixed cobordism.

The smooth-core version of this translation is described in [ISST, Section 4, equation (20)]. The partial marking is checked below, and the web compactification is treated in Section 7. The singular local filling never crosses the Hopf surgery, and the translation preserves its facets, dots and prescribed normal collars.

Fix the bundle and the gauge subgroup on the excision core before making this translation. Within the spectator region retain the ordinary partial marking of p_j. In particular, do not enlarge the marking across the whole complement of Q and then require its classes to extend over an arbitrary P_j. That stronger extension condition is neither given nor needed.

The ordinary filling factor at either limiting composition has product Hopf-tube marking. On each connected component its marking domain minus the singular set is the product of an interval with a Hopf-ball complement. Restriction to either endpoint is consequently an isomorphism on H^0 and H^1 over $\mathbb{F}_2$. It is both left- and right-proper in the sense of [KM1, Definition 3.5]. These proper factors supply the Mayer–Vietoris condition of [KM1, Proposition 3.4]; one need not assert properness for an isolated excision block with disconnected ends. The additional finite core quotient remains part of the auxiliary map.

For clarity, an elementary endpoint calculation explains why the core marking does not introduce new ordinary critical generators. Let H be the Hopf link in a ball B_H and let $B_1, \dots, B_m$ be spectator balls, where $m = 1$ or 2. Set

$$M_m = S^3 \setminus \big(H \cup \textstyle\bigcup_a \operatorname{int} B_a\big), \qquad U_H = B_H \setminus H.$$

Attaching the simply connected region outside B_H along its boundary sphere shows that restriction gives an isomorphism

$$H^1(M_m; \mathbb{F}_2) \xrightarrow{\cong} H^1(U_H; \mathbb{F}_2) = \mathbb{F}_2^2. \tag{4.4}$$

Hence the marking enlargement has zero covering kernel, by [KM1, Lemma 2.4]. The ranks of H^2 are $m + 1$ and 2, respectively. For $m = 2$ the extra bundle choice is detected by the sphere separating the two spectator balls. Fix its w_2 evaluation to be zero. Every flat connection has this value, since a flat bundle on S^2 is trivial. Compactness of the small-perturbation critical set excludes critical points in the other sphere sector for sufficiently small perturbations. This verifies the endpoint identification; it is not a claim that all marking classes extend across all local fillings.

The subgroup for a disconnected composition must include its Mayer–Vietoris classes. The explicit calculation in Section 4.3 specifies this subgroup and its restrictions at all ordinary and torus ends.

4.3 A geometric inverse and the correlated torus ends

Next we compare the composite of the excision cobordism and its reverse with the product cobordism. At the chain level we need a homotopy H_{exc} satisfying

$$\delta H_{\mathrm{exc}} = VV' + 1_{E\otimes U}. \tag{4.5}$$

As with the preceding comparison, an inverse on homology is not enough: we need to know the cobordisms on which the homotopy counts instantons. The geometric comparison cuts the composite along a three-torus and fills its two new boundary components with copies of $T^2 \times D^2$. There is a marking issue in making this comparison. Each torus end has two critical lifts, but the allowable change of marking exchanges the two lifts at both ends at once. We must therefore keep track of the pair of lifts, rather than identify the two lifts independently at each end. We give the marking calculation first.

The excision cobordism and its marking. Write $W_H, \overline{W}_H$ for the forward and reverse Hopf-excision cores, X_c for their composite, $N = T^2 \times S^1$ for its internal torus, and X_p for the result of cutting there and inserting two $T^2 \times D^2$ caps. Let Z_{cut} be the common cut exterior. The ordinary incoming and outgoing manifolds each have two three-sphere components, including the retained empty-web factor.

The excision block is described by $T^2 \times \mathcal{U}$, where $\mathcal{U}$ is a disk with corners. The four solid-torus pieces attached to its sides contain the Hopf annuli. After deleting those annuli, their complements are torus collars extending the sides of $\mathcal{U}$. Deleting the spectator $B^3 \times I$ tubes does not change H^1, by Mayer–Vietoris with intersection $S^2 \times I$. Thus the marking-domain complement has the same H^1 as $T^2 \times \mathcal{U}$. Ordinary end restriction identifies its two H^1 generators with the Hopf meridians. The underlying disk and spectator construction are the excision model of [KM4, proof of Theorem 5.6] and [ISST, Section 4].

Gluing $\mathcal{U}$ to its reverse along the two intermediate intervals produces an annulus $\mathcal{A}$. Use inverse torus identifications on the reverse core; there is no torus monodromy around $\mathcal{A}$. If z denotes its angular class, the composite marking complement, denoted C_c, has

$$H^1(C_c; \mathbb{F}_2) = H^1(T^2; \mathbb{F}_2) \oplus \mathbb{F}_2 z.$$

Cutting the central circle gives two annuli $\mathcal{A}_1, \mathcal{A}_2$ and sends z to (z_1, z_2). Each z_i restricts to ds on its torus boundary and to zero on every ordinary end. Filling the central boundary circle by a disk kills z_i.

The cohomology of the marking complement is not the same as the cohomology that specifies the additional finite quotient by changes of marking. For the latter we use the ambient cobordism. The individual four-ended core has $H^1(W_H; \mathbb{F}_2) = 0$, as does its reverse. The two-component intermediate boundary gives one Mayer–Vietoris class c on the composite:

$$H^1(X_c; \mathbb{F}_2) = \mathbb{F}_2 c, \qquad H^1(X_p; \mathbb{F}_2) = 0.$$

The class c evaluates to one on the core loop crossing the two different intermediate components, so it restricts to z in the marking complement. It is precisely the extra class needed for composition

across that disconnected boundary. Writing Γ for this finite group on each of the indicated pieces, we obtain

$$\Gamma_{W_H} = \Gamma_{\overline{W}_H} = 0, \quad \Gamma_c = \mathbb{F}_2 c, \quad \Gamma_{\mathrm{cut}} = \mathbb{F}_2(z_1, z_2), \quad \Gamma_p = 0. \tag{4.6}$$

Their restrictions to ordinary external ends are zero in the ordinary marking quotient. This follows also by restriction through $H^1(S^3; \mathbb{F}_2) = 0$.

More explicitly, in the complement basis (x_i, y_i, z_i) the ordinary restriction has matrix $\left(\begin{smallmatrix} 1 & 0 & 0 \\ 0 & 1 & 0 \end{smallmatrix}\right)$, up to the fixed meridian interchange, and torus restriction is the identity. After capping, only (x_i, y_i) remain and ordinary restriction is injective. In ambient cohomology, restriction across N is $(a, b) \mapsto (a + b)ds$, whose kernel is the diagonal. These matrices also show that no further endpoint-trivial partial-marking kernel survives on the product side. The fixed product coordinates are used: the meridian coefficient alone would not rule out extra dx, dy terms after an arbitrary change of torus framing.

The capped manifold X_p has two product components. A connected cap attached along one connected boundary cannot join two components of Z_{cut}. It follows that $Z_{\mathrm{cut}} = Z_1 \sqcup Z_2$, with each Z_i carrying the ordinary strong ends of its product component. In particular N separates X_c. Its absolute dual in $H^1(X_c; \mathbb{F}_2)$ is zero. The nonzero class c above is the disconnected-composition class, not the dual of this separating cut. Consequently the general trace hypothesis involving the class dual to the cut imposes no further condition in this topology.

Fix the flat bundle P_T on T^2 with orthogonal half-turn holonomies. Use its product pullback over $\mathcal{U}$, its reverse, and both caps. The gluing identifications are fixed to agree with this one reference. On N this gives

$$w_2(P_N) = \mathrm{pr}_{T^2}^* \, w_2(P_T);$$

both mixed two-torus evaluations are zero. The third holonomy of the flat connection is the identity. This specification is needed: merely requiring nonzero $w_2[T^2]$ would leave other sectors.

The spectator region is excluded from this marking. Thus this core construction preserves the ordinary marking, proper factors and framed arcs of the translation in (4.3).

We also need to realize the class z by a change of the marking isomorphism, rather than merely record it in cohomology. This change is made on the Hopf core; it need not extend as a gauge transformation across the spectator foam. For existence, let L_z be the real line bundle with $w_1(L_z) = z$. A unit section of $L_z \otimes (\mathbb{R} \oplus E_\mu)$ supplies local unit quaternions whose conjugations patch to a marking automorphism with lift obstruction z. The first obstruction is in $H^4(C_c; \mathbb{Z})$, which vanishes for this core with boundary, and there are no higher obstructions in dimension four. Its square is liftable. This realizes the indicated order-two deck action without imposing a new condition on the spectator foam.

Retaining the two torus lifts jointly. In the specified bundle sector on N, the flat critical point has two lifts when we take the quotient by determinant-one gauge transformations. Denote them by t_0, t_1. The angular gauge class ds exchanges them. Each is acyclic: the cohomology with coefficients in its adjoint local system is zero. Indeed, that local system is a sum of three real characters, each nontrivial on T^2. The same argument proves acyclicity on $T^2 \times D^2$.

On the pair of oppositely oriented torus boundaries, the restriction of (4.6) acts by

$$(t_i, t_j) \longmapsto (t_{i+1}, t_{j+1}).$$

Thus the four ordered pairs of critical lifts give two orbits. The complex for the pair of torus boundaries, with this quotient, is

$$\mathcal{T}_\Delta = \mathbb{F}_2 \mathfrak{a} \oplus \mathbb{F}_2 \mathfrak{b}, \qquad \mathfrak{a} = [00] = [11], \quad \mathfrak{b} = [01] = [10]. \tag{4.7}$$

It has zero differential: the two orbits differ in grading by four and admit no index-one trajectory. One may equivalently begin with the two perfect determinant-one torus complexes and take their diagonal quotient. Quotienting them separately would also identify $\mathfrak{a}$ with $\mathfrak{b}$, which the geometry does not permit.

Lemma 4.1 (The matching torus limits)**.** *Use the same exterior metric, equation, dot data and relative sectors on Z_{cut}, with perturbations and cuts invariant under the indicated marking quotient. Let $\mathcal{X}_{ij}$ be its moduli problem with determinant-one torus limits (t_i, t_j), before the extra finite quotient. Let G be that extra quotient and G_0 the kernel of its boundary-lift action. If its image is the diagonal exchange, then*

$$(\mathcal{X}_{00} \sqcup \mathcal{X}_{11})/G \;\cong\; \mathcal{X}_{00}/G_0. \tag{4.8}$$

For (4.6)*, $G = \Gamma_{\mathrm{cut}}$ and $G_0 = 0$. With the fixed product cap framings, the composite cylinder and the two caps select the left and right sides of* (4.8)*, respectively.*

Proof. The generator is an actual marking-deck transformation induced by $c|_{Z_{\mathrm{cut}}}$. It exchanges $\mathcal{X}_{00}$ and $\mathcal{X}_{11}$ and preserves the equation and cuts. Each matching orbit has exactly one representative in $\mathcal{X}_{00}$, modulo G_0. This proves the bijection before counting. It is not division of a mod-two count by two.

The flat cylinder has matching lifts 00 and 11, interchanged by its extending angular class. It selects the matching orbit $\mathfrak{a}$ once. The product flat cap pair has the single lift 00 in the chosen boundary framings. The class ds cannot extend across a disk cap. Consequently the group extending across both caps is exactly G_0, and the pair selects the right side of (4.8). Both cap framings have been aligned with the same P_T reference; changing only one of them would select the other orbit.

There is no further determinant-central multiplicity. The incidence graph for the original $W_H, \overline{W}_H$ composition has two vertices and two edges, and its one-dimensional H^0 Mayer–Vietoris cokernel is exactly the included class c. The torus-cylinder decomposition has graph Z_1–cylinder–Z_2, a tree. The cap decompositions have two disjoint single-edge graphs. Their corresponding cokernels are zero. This is the central-lift issue in the composition convention of [KM4, Propositions 5.4–5.5]. □

The bijection is induced by marking-deck transformations on a fixed exterior; these cover the same underlying connection problem. It preserves curvature action, index and cut-down data. Both local fillings are flat and have zero action. No trajectory switching t_0 and t_1 is inserted.

The common term in the two neck-stretching limits. Let

$$Q_{\mathfrak{a}}, Q_{\mathfrak{b}} : E \otimes U \longrightarrow E \otimes U$$

be the operations obtained by counting on the cut exterior with the torus boundary condition $\mathfrak{a}$ or $\mathfrak{b}$, respectively. The preceding lemma says that the flat cylinder and the two flat caps both give the term $Q_{\mathfrak{a}}$. Let W_c and W_p be the maps of the composite and product cobordisms before stretching the torus necks. The four comparison homotopies then satisfy

$$\delta H_{\mathrm{comp}} = VV' + W_c, \tag{4.9}$$
$$\delta H_{\mathrm{cut},c} = W_c + Q_{\mathfrak{a}}, \tag{4.10}$$
$$\delta H_{\mathrm{cut},p} = W_p + Q_{\mathfrak{a}}, \tag{4.11}$$
$$\delta H_{\mathrm{cont}} = W_p + 1. \tag{4.12}$$

Each line has one parameter on a fixed cobordism: ordinary composition, neck stretching on the composite, simultaneous neck stretching at the two product caps, and product continuation. The two middle broken terms agree by Lemma 4.1. Proposition 7.6 proves that they are the full torus ends in the dimensions being counted, including the one-parameter diagonal of the two cap neck lengths.

Their sum is H_{exc} and satisfies (4.5). The operation $Q_{\mathfrak{b}}$ is retained in the joint boundary model; neither flat filling selects it, and no vanishing assertion about it is needed. The replacement pieces $T^3 \times I$ and $T^2 \times D^2$ are smooth and disjoint from the foam. This comparison changes no dot, normal framing or parameter count. Its topological excess is computed in Proposition 6.4.

Proposition 4.2 (Geometric comparison families)**.** *For the finite collection of local relations below, the identities* (4.1), (4.3) *and* (4.9)–(4.12) *can be realized by the indicated marked cobordisms and one-parameter families with shared endpoint data. The local complexes are the actual perfect complexes used for the relative chains p_j. On each common broken face, the metric, perturbation, bundle restriction, marking quotient and dot data agree.*

The zero- and one-dimensional cut-down spaces are regular. Their ends are the stated parameter limits, ordinary Floer breakings and the even local tetrahedral bubble branches of the bifold construction. The torus limits use the matching coefficient $Q_{\mathfrak{a}}$ with multiplicity one. Moreover, for any $\varepsilon > 0$, the data can be chosen so that the total perturbation error in the action estimate for each complete capped term is less than ε, as in Theorem 7.8.

Proof. The constructions above specify the collared cobordisms, the actual subgroups and their restrictions, the bundle sectors and the flat matching terms. Ordinary fillings are proper at the required cuts. Every ordinary comparison component, including each component of Z_{cut}, retains a strongly marked ordinary end. The only additional isolated pieces are the torus cylinder and caps.

The analytic proof is supplied in Section 7: Proposition 7.3 gives universal surjectivity by varying additional time-dependent perturbations on ordinary end collars, with the endpoint complexes fixed; Proposition 7.6 gives the torus compactification and its gluing charts. The relative choice argument and quantitative bounds in Theorem 7.8 then select one shared collection of data. That argument uses the explicit geometries above and their common boundary faces, not the localization identity or the value of any scalar coefficient. Thus it introduces no circular dependence on the algebraic consequences proved next. □

4.4 The chain homotopy for a local relation

We can now combine the preceding comparisons. The formula below has three terms for each filling: the composition homotopy, the homotopy that moves the filling past excision, and the homotopy that cancels excision with its reverse. Keeping the one-generator complex U in the formula makes the domains and codomains explicit.

Proposition 4.3 (The localization chain homotopy)**.** *Use the geometric comparison maps of Proposition 4.2. Define a map on $E \otimes U$ by*

$$\widetilde{K} = \sum_j \left(R_j \otimes 1_U + (O \otimes 1_U) N_j V' + (OL_j \otimes 1_U) H_{\mathrm{exc}} \right). \tag{4.13}$$

Then

$$\delta \widetilde{K} = \sum_j F_j \otimes 1_U + (O \otimes 1_U) \Psi_{K,Q} \left(1_E \otimes \sum_j p_j \right) V'. \tag{4.14}$$

In particular, if $\sum_j p_j = 0$ *as actual chain maps* $U \to D$*, the identification* $U = \mathbb{F}_2 u_\varnothing$ *gives a homotopy* K_{loc} *with* $\delta K_{\mathrm{loc}} = \sum_j F_j$*. Every constituent of* (4.13) *has exactly one family parameter.*

Proof. All fixed cobordism maps are δ-closed. Apply the Leibniz rule and the three identities to obtain, for each j,

$$\begin{aligned}
\delta\big(R_j \otimes 1_U\big) &= F_j \otimes 1_U + OL_j \otimes 1_U,\\
\delta\big((O \otimes 1_U)N_j V'\big) &= (O \otimes 1_U)\Psi_{K,Q}(1_E \otimes p_j)V' + (OL_j \otimes 1_U)VV',\\
\delta\big((OL_j \otimes 1_U)H_{\mathrm{exc}}\big) &= (OL_j \otimes 1_U)VV' + OL_j \otimes 1_U.
\end{aligned}$$

The repeated terms cancel over $\mathbb{F}_2$. Summing proves (4.14). The identification with K_{loc} is an identification of linear map spaces; it is not a claim that each underlying cobordism is a product with an empty factor. Only R_j, N_j or one summand of H_{exc} varies in each constituent. All other factors are fixed, so no second parameter is introduced. □

If $d_D = 0$, equality of the relative invariants $\sum_j [p_j] = 0$ implies $\sum_j p_j = 0$ literally. This is why the local complex must be a genuine zero-differential Floer complex. If instead we replaced D by its homology using an arbitrary chain equivalence, the comparison would introduce further homotopies for which we had not specified any cobordisms. The relation is used over $\mathbb{F}_2$; no equality of action-weighted relative invariants is asserted.

4.5 The local relations used below

We apply this construction to four kinds of local relation. To find the boundary web Q, enclose the local foam in a four-ball and inspect its intersection with the boundary sphere. In the present cases this amounts to doubling the corresponding tangle. The results are:

Relation	Local boundary	Occurrences
Square decomposition	Cube	4
Triangle-side inverse	Triangular prism L_3	13
Source comparison, A component	Theta	1
Source comparison, B component	Handcuff	1

For the triangle relation, let T be the triangle tangle with three external legs and Y the three-legged star. Doubling Y gives theta; doubling T gives L_3. The star-side composite and the triangle-side composite therefore require different local complexes. The two relative relations are the fillings in [KM1, Figures 10–11 and Proposition 6.6]. A rank-six identification alone cannot exchange these boundaries.

For the source comparison, the local incoming tree has two vertices joined by one edge and exterior pairs $(9, 11)$ and $(10, 2)$. The A smoothing pairs $(9, 10)$ and $(2, 11)$. Both smoothing arcs join the two vertices in the doubled boundary, yielding theta. The B smoothing pairs $(9, 11)$ and $(10, 2)$; each arc gives a loop at one vertex, leaving a connecting bridge. Its boundary is the handcuff. The latter has no flat connection: a sphere meeting the bridge once makes the bridge meridian trivial, while bifold holonomy requires a nontrivial half-turn. Thus it has an empty complex for sufficiently small perturbations.

The theta source filling has the collapsed-side triangle comparison. The three seam paths between its two tetrahedra are, in the labelled local movie,

$$t_1\text{–}!20\text{–}!t_2, \qquad t_1\text{–}!22\text{–}!24\text{–}!t_2, \qquad t_1\text{–}!23\text{–}!25\text{–}!t_2.$$

The intervening facets are the prescribed planar disks, so this is the relative filling of Figure 10, with its specified collars. Its equality with the ordinary source filling is a relative theta relation. In an actual perfect theta complex it is a literal chain equality. The handcuff relative chain is zero in the empty complex. Application of Proposition 4.3 therefore gives the two components of

$$\delta L_H = P_X \widehat{H} I_Z + (s, 0),$$

with the common geometric data of Proposition 4.2. The fourth square relation gives $\delta T_X = 1 + I_X P_X$. These are the transfer homotopies used by the normalized scalar formula.

4.6 Combining the reductions of K_0

Recall that the two cycles c_1, c_3 used in the finite calculation have $[sc_1] = [sc_3] = 0$. Thus each sc_i is a boundary. We now construct a single operator T_A such that $T_A sc_i$ is a primitive for this boundary: $d(T_A sc_i) = sc_i$. The point of using the reductions of K_0 is to express T_A as a sum of the geometric homotopies already described.

Let $A = CF^\sharp(K_0)$, with the two facial square reductions at $(2, 3, 13, 11)$ and $(8, 9, 10, 18)$ in the labelled web. The second reduction is made on both branches of the first. Write

$$P_i : A \to A_i, \quad I_i : A_i \to A, \qquad Q_{ij} : A_i \to A_{ij}, \quad J_{ij} : A_{ij} \to A_i \quad (i, j \in \{0, 1\}).$$

The four subsequent routes contain $2, 4, 4, 3$ triangle collapses, respectively. Denote their composite collapses and reverse maps by

$$R_{ij} : A_{ij} \to D_{ij}, \qquad S_{ij} : D_{ij} \to A_{ij}.$$

The terminal webs are a double-bigon theta, theta, theta and L_2, with actual zero-differential complexes of dimensions $24, 6, 6, 12$, respectively, as constructed in Proposition 3.1.

Let K, L_i and T_{ij} be the geometric homotopies supplied by Proposition 4.3, so that

$$\delta K = 1 + \sum_i I_i P_i, \qquad \delta L_i = 1 + \sum_j J_{ij} Q_{ij}, \qquad \delta T_{ij} = 1 + S_{ij} R_{ij}. \tag{4.15}$$

The last homotopy is obtained by combining the successive triangle relations. If $r_k : A_{k-1} \to A_k$ and $s_k : A_k \to A_{k-1}$ are successive triangle maps and $\delta h_k = 1 + s_k r_k$, then

$$T = h_1 + s_1 h_2 r_1 + \cdots + s_1 \cdots s_{m-1} h_m r_{m-1} \cdots r_1$$

satisfies $\delta T = 1 + (s_1 \cdots s_m)(r_m \cdots r_1)$. Indeed, the terminal term of each summand cancels the initial term of the next. Every summand still has one parameter.

Proposition 4.4 (Common source primitive)**.** *With the actual maps and homotopies in* (4.15)*, set*

$$T_A = K + \sum_i I_i L_i P_i + \sum_{i,j} I_i J_{ij} T_{ij} Q_{ij} P_i,$$
$$\Pi = \sum_{i,j} I_i J_{ij} S_{ij} R_{ij} Q_{ij} P_i.$$

Then $\delta T_A = 1 + \Pi$. If $z \in A$ is a boundary and every D_{ij} has zero differential, then $\Pi z = 0$ and $d(T_A z) = z$.

Proof. The differential of the first summand contributes $1 + \sum_i I_i P_i$. The second contributes $\sum_i I_i P_i + \sum_{i,j} I_i J_{ij} Q_{ij} P_i$. The third contributes $\sum_{i,j} I_i J_{ij} Q_{ij} P_i + \Pi$. Cancellation gives the operator identity. Write $z = da$. Since $R_{ij} Q_{ij} P_i$ is a chain map, its value on z is $d_{D_{ij}}(R_{ij} Q_{ij} P_i a) = 0$. Hence $\Pi z = 0$. Finally $dz = 0$ gives $dT_A z = (1 + \Pi) z = z$. □

Apply this proposition to $z = sc_1$ and $z = sc_3$. The finite computation says that the full cycles c_1, c_3 lie in $\ker H(s)$, so these full images are boundaries. Individual half-foam summands need not be in that kernel. The same T_A works for both sources, and the construction asserts neither $\Pi = 0$ nor a contraction of the entire complex A.

For later use, the primitive on the augmented all-L complex is

$$\widehat{x} = T_X \widehat{H} I_Z c + I_X \big(L_H c + (T_A sc, 0) \big). \tag{4.16}$$

Differentiation, before using the terminal vanishing, gives

$$d\widehat{x} = \widehat{H} I_Z c + I_{X,A} \Pi sc.$$

Proposition 4.4 removes the residual term. Thus $d\widehat{x} = \widehat{H} I_Z c$. This is the primitive used in the normalized secondary operation of the next section. Its construction adds no dots. Each expanded term contains one of the comparison families described here, surrounded by fixed maps; its capped topology is the subject of Proposition 6.4.

5 The secondary operation and its normalization

The definition of h in Section 2 is a diagram chase: for a class $[c] \in \ker s$, choose a class $u \in J^\sharp(K_2)$ with $r(u) = [c]$, apply b, and take its image in $\operatorname{coker} \gamma$. To use an index calculation we need to express this procedure as a count on specified cobordisms and one-parameter families. The primitive constructed in the preceding section provides one part of this expression. The other part is the chain homotopy used in the proof of the exact triangle.

There is a normalization to check. A chain homotopy between a composite map and zero does not by itself ensure that the class it produces maps back to $[c]$ under r. For the particular families in [KM2, Sections 6–8], this follows from the two-parameter pentagon and the identification of one of its boundary operations with the identity. We will spell out that argument and thereby identify our geometric count with the map h already defined.

In this section the geometric maps and homotopies are assumed to satisfy the indicated boundary identities. Theorem 7.8 constructs compatible auxiliary data for them. The algebra below states precisely how those identities are used.

5.1 Conventions and geometric reductions

For complexes over $\mathbb{F}_2$, write $\delta U = dU + Ud$ for the differential on a space of maps. All sums and formulas below are in characteristic two. We do not impose an absolute integer grading on $J^\sharp$; the dimension of each parametrized moduli space is supplied separately by its deformation index.

We use the exact triangle in which all three local webs are of L-type, calling it the *all-L triangle* to distinguish it from the triangles involving two K-type webs. Write its geometric complexes and cobordism maps as

$$\widehat{Z} \xrightarrow{\widehat{H}} \widehat{X} \xrightarrow{\widehat{F}} \widehat{Y} \xrightarrow{\widehat{G}} \widehat{Z}.$$

Choose the cyclic order so that the local reductions give

$$X = A \oplus B, \qquad Y = W \oplus B, \qquad Z = C.$$

The hats distinguish the complexes before these local reductions. The complexes without hats are the geometric Floer complexes on the reduced webs; we have not replaced them by their homology. The triangle expansion and collapse give maps $I_Z : C \to \widehat{Z}$ and $P_Z : \widehat{Z} \to C$. Similarly, the two square resolutions give maps I_X, P_X, I_Y, P_Y between the other complexes and the displayed direct sums. These are the geometric maps inducing the isomorphisms on homology in [KM2, Section 8]. In the notation of the split diagram in [KM2, Section 8], the cyclic relabelling is

$$K_2^{\text{printed}} \mapsto K_0, \quad K_1^{\text{printed}} \mapsto K_2, \quad K_0^{\text{printed}} \mapsto K_1, \quad L_0^{\text{printed}} \mapsto L_1.$$

On homology, therefore, the three maps become $(s,0)^t$, $\mathrm{diag}(a, 1_B)$ and $(r,0)$, respectively. The crossing conventions for the embedded foams are specified in Section 6.

In particular, the comparison in [KM2, Section 8] gives

$$H(P_Z I_Z) = 1, \qquad H(I_Y P_Y) = 1, \qquad H(P_Z \widehat{G} I_Y) = (r,0). \tag{5.1}$$

Using $H(I_Y P_Y) = 1$ in the last identity also gives

$$H(P_Z \widehat{G}) = (r,0) H(P_Y). \tag{5.2}$$

No chain-level equality between the transported map $\widehat{G}$ and $(r,0)$ is required.

5.2 A primitive on the unreduced complex

We begin with a source cycle $c \in C$ for which $[sc] = 0$. To carry out the diagram chase on the all-L triangle, we need a chain $\widehat{x} \in \widehat{X}$ with $d\widehat{x} = \widehat{H} I_Z c$. We obtain it by transporting the primitive $T_A sc$ through the local reductions, keeping the comparison homotopies explicitly.

Suppose, as in Section 4, that geometric homotopies T_X and L_H have been chosen with

$$\delta T_X = 1 + I_X P_X, \qquad \delta L_H = P_X \widehat{H} I_Z + (s,0)^t. \tag{5.3}$$

The first uses the square relation; the second has a theta local boundary on its A component and a handcuff local boundary on its B component. Their geometric construction is included in Section 4. We use these equalities for the geometric chain maps themselves; knowing only the corresponding identities on homology would not suffice for the following formula.

Let c be either of the full source cycles c_1, c_3 specified in Section 2. The terminal reductions there and in Section 4 give

$$\delta T_A = 1 + \Pi, \qquad \Pi sc = 0. \tag{5.4}$$

In particular $y = T_A sc$ satisfies $dy = sc$. Define

$$\widehat{c} = I_Z c, \qquad \widehat{x} = T_X \widehat{H} \widehat{c} + I_X \big(L_H c + (T_A sc, 0)^t \big). \tag{5.5}$$

Lemma 5.1. *Under* (5.3) *and* (5.4), $d\widehat{x} = \widehat{H}\widehat{c}$.

Proof. Since c is a cycle and all I, P, H, s maps in this calculation are chain maps, differentiating (5.5) gives

$$\begin{aligned} d\widehat{x} &= \widehat{H}\widehat{c} + I_X P_X \widehat{H}\widehat{c} + I_X \big(P_X \widehat{H} I_Z c + (sc,0)^t \big) + I_X \big(sc + \Pi sc, 0 \big)^t \\ &= \widehat{H}\widehat{c} + I_X (\Pi sc, 0)^t. \end{aligned}$$

The last term vanishes by (5.4). Only its value on the full source c is used. It need not vanish on an individual half-foam summand. □

5.3 Normalization by the pentagon

In the proof of the all-L exact triangle, the composite of two successive foam cobordisms is equipped with a one-parameter family of metrics. One end stretches along the intermediate web; the other stretches along a local three-sphere. The associated map $\widehat{J} : \widehat{Z} \to \widehat{Y}$ satisfies $\delta\widehat{J} = \widehat{F}\widehat{H}$. For the next pair of cobordisms in cyclic order there is a corresponding map J_{GF} with $\delta J_{GF} = \widehat{G}\widehat{F}$.

The two-parameter family over the pentagon compares these nullhomotopies. Together with the calculation on its special face, it gives a further chain homotopy R satisfying

$$\delta R = \widehat{G}\widehat{J} + J_{GF}\widehat{H} + 1_{\widehat{Z}}. \tag{5.6}$$

Indeed, the pentagon boundary formula in [KM2, Section 6, equation (12)] has two ordinary composition faces, two sphere faces and the $S^{2,1}$ face. The sphere terms vanish by the stated connected-sum calculation, and Section 7 identifies the special-face operation up to chain homotopy with the identity. Combining that homotopy with the pentagon gives (5.6).

Proposition 5.2 (Normalized cycle formula)**.** *Assume that the actual geometric families satisfy* (5.6)*, that* (5.1) *holds, and that $\widehat{x}$ is as in Lemma 5.1. Let ℓ be an actual cap cocycle on B whose homology functional annihilates* $\operatorname{im}\gamma$*. Then*

$$\ell h([c]) = \widehat{q}\big(\widehat{J}\widehat{c} + \widehat{F}\widehat{x}\big), \qquad \widehat{q} = \ell b \operatorname{pr}_W P_Y. \tag{5.7}$$

Proof. Set $\widehat{w} = \widehat{J}\widehat{c} + \widehat{F}\widehat{x}$. The identity $\delta\widehat{J} = \widehat{F}\widehat{H}$ and $d\widehat{x} = \widehat{H}\widehat{c}$ imply $d\widehat{w} = 0$. Applying the normalization identity (5.6) to this cycle gives

$$\widehat{G}\widehat{w} = \widehat{c} + d\big(R\widehat{c} + J_{GF}\widehat{x}\big). \tag{5.8}$$

To check it, apply (5.6) to $\widehat{c}$, and apply $\delta J_{GF} = \widehat{G}\widehat{F}$ to $\widehat{x}$; the two $J_{GF}\widehat{H}\widehat{c}$ terms cancel.

Let u be the W component of $H(P_Y)[\widehat{w}]$. Applying $H(P_Z)$ to (5.8) and using (5.2) yields $r(u) = [c]$. By the definition of the secondary map, $h([c]) = b(u) \bmod \operatorname{im}\gamma$. Evaluating with ℓ proves (5.7). Its independence of the lift u follows from $ba = \gamma$ on homology, exactly as in the definition of h. □

Remark 5.3. The identity term in (5.6) is what ensures that the class u maps to $[c]$, rather than to its image under an unspecified automorphism. Merely knowing that a cone comparison is a quasi-isomorphism would leave this ambiguity. There is a related ambiguity in choosing $\widehat{J}$: two solutions of $\delta\widehat{J} = \widehat{F}\widehat{H}$ differ by a cycle in the mapping complex, and its contribution to (5.7) need not vanish. Finally, $\widehat{x}$ need not be a cycle. If we replace $\widehat{F}$ by a chain-homotopic map when evaluating it on $\widehat{x}$, we must include the correction from that homotopy. Formula (5.7) avoids these ambiguities by using the specified normalized family and the original chain map $\widehat{F}$.

5.4 Which families enter the action estimate

Substitution of (5.5) into (5.7) gives four types of term:

$$\begin{aligned} &\widehat{q}\widehat{J}I_Z c, \qquad \widehat{q}\widehat{F}T_X\widehat{H}I_Z c, \\ &\widehat{q}\widehat{F}I_X L_H c, \qquad \widehat{q}\widehat{F}I_X(T_A sc, 0)^t. \end{aligned} \tag{5.9}$$

Substitute into T_A, T_X, L_H the expressions in Section 4. Each resulting summand is a count on a composition of fixed cobordisms with just one cobordism carrying a one-parameter family. Attach the source filling and the cap specified by ℓ to obtain the corresponding closed foam. The dots on

these fillings remain in place, and the construction introduces no new dots. The two evaluations using ℓ_2 have three dots in total. Each of the two fixed cap summands of the evaluation using ℓ_1 has two. Although the latter summands can be counted separately within this chosen expansion, only their sum defines a functional on $\operatorname{coker}\gamma$.

The estimate in Section 7 will be applied to the complete capped terms in (5.9). It bounds how far the perturbations can lower their topological action. The map R, the interior of the pentagon, and the homotopy identifying the $S^{2,1}$ operation with the identity do not occur in these terms. They establish the normalization, so they must be compatible with the counted families, but they do not themselves need to satisfy this small bound on the action error. Theorem 7.8 preserves this distinction.

We must make these choices in the right order. First fix the families of metrics used in the published construction, including the local sphere models, the allowed family on $S^{2,1}$, and their common restrictions at the corners. Only then choose the additional perturbations for the family $\widehat{J}$ that enters the count. These perturbations are supported on collars of the ordinary external ends, away from the isolated local pieces. The two faces corresponding to ordinary composition therefore use the same maps at their common corners, and their sphere limits agree with the local models already chosen.

Theorem 7.8 extends the choices over the remaining families while preserving these restrictions. The available generic metrics are those of [KM2, Proposition 7.1]; we do not assert such an extension for an arbitrary local model chosen in advance. This order of choices keeps the normalization required in Proposition 5.2.

6 The index calculation for the closed foams

The three scalar expressions in the preceding section are counts of configurations on composites of foam cobordisms. A source foam closes the incoming web and a cap closes the outgoing web. After identifying the remaining marked ends, each composite determines a closed bifold. We shall compute the topological term in its ASD index formula. The answer, together with the number of dots and the one metric parameter, will force any contributing configuration to have negative action. Section 7 will exclude that possibility by an estimate for small perturbations.

For this calculation, the choice of chain homotopy matters. A relation between maps on homology does not specify the topology of a family realizing that relation. We use the particular foam cobordisms and families described in Proposition 4.2, keeping their normal framings and the auxiliary four-manifolds introduced by excision. The topological calculation can be made before choosing regular perturbations; the compatible analytic choices are supplied later by Theorem 7.8.

6.1 Conventions for normal numbers and gluing

For a foam Σ in an oriented four-manifold, write $\nu(\Sigma)$ for the self-intersection number of [KM1, Definition 2.5], and let $\tau(\Sigma)$ be its number of tetrahedral points. Thus ν is *half* the relative Euler number of the squared normal bundle of the normalized facets, with the canonical seam section. Put

$$Q(\Sigma) = \chi(\Sigma) + \tfrac{1}{2}\nu(\Sigma) - \tfrac{1}{2}\tau(\Sigma), \qquad I_{\mathrm{top}}(X,\Sigma) = -\tfrac{3}{2}\big(\chi(X)+\sigma(X)\big) + Q(\Sigma). \tag{6.1}$$

The closed deformation index is $8\kappa + I_{\mathrm{top}}$ by [KM1, Proposition 2.6]. Formula (6.1) is additive over connected components. In particular, no fixed value of $b_0(X)$ is implicit when an auxiliary component is introduced.

For relative comparisons all boundary collars and their normal sections are fixed. Gluing foams along a web K subtracts $\chi(K)$ from their summed Euler characteristics. The normal obstructions

add when the prescribed sections are identified; this condition is part of our gluing convention. We write $\Delta(\chi, \nu, \tau)$ for the difference between two fillings of the same collared boundary. Such a notation is used only after an actual relative geometric comparison has been specified.

Lemma 6.1 (A hypersurface normal section)**.** *Suppose that a closed foam Σ is contained in an oriented embedded three-manifold M in an oriented four-manifold, and that its seam and vertex models are the standard models in M. Then $\nu(\Sigma) = 0$.*

Proof. Let F be a normalized facet and N_F its ambient normal bundle. The line bundle $N_M F \subset N_F$ gives a nowhere-zero section of $N_F^{[2]}$: the images of the two unit vectors in a fiber coincide in the squared bundle. This construction does not require F to be orientable. At its boundary, the three-plane used to define the canonical seam section is TM. The section just constructed consequently restricts to that canonical section. It has zero relative Euler obstruction. The same statement holds after rounding the standard tetrahedral corners in M, and summing over the normalized facets proves the claim. □

6.2 A reference closed foam

We begin with a simpler composite, using the standard planar maps s and γ. Its index can be calculated directly from the reduction foams in Section 2. We will then compare each composite that occurs in the scalar formula with this reference foam. All the comparisons are made relative to fixed boundary collars, so that the normal numbers can be compared as well as the Euler characteristics.

Use the spherical embedding of the generalized Petersen graph $G(10, 2)$, with edges

$$\{i, i+1\}, \quad \{i, 10+i\}, \quad \{10+i, 10+(i+2)\}, \qquad i \in \mathbb{Z}/10.$$

The integer additions in the first and third families are taken modulo ten within their respective sets of ten vertices. Remove vertices $0, 1$ and their incident edges. The remaining exterior has four ends in cyclic order $(9, 10, 2, 11)$. The webs K_0, K_1, L_1 used for A, B, C are obtained by inserting, respectively,

$$\begin{aligned} K_0 &: \ (9,10),(2,11), \\ K_1 &: \ (9,11),(10,2), \\ L_1 &: \ (20,21),(20,9),(20,11),(21,10),(21,2). \end{aligned}$$

These insertions use one common disk and the inherited spherical rotation system. In particular, the two adjacent matchings are not identified by an unspecified permutation of their external ends.

Recall how the basis foams were constructed. Reduce a web by bigon, triangle and square moves supported in faces of its planar diagram, and finish by filling the resulting theta web. Each step is a standard foam cobordism. The resulting foam, or its reflection with the direction of the cobordism reversed, supplies a cap or a source respectively. A square branch specifies one of its two adjacent pairings. At each stage use the standard untwisted local foam in the indicated face disk times an interval and the product on its complement. The triangle and square models are those of [KM1, Figures 10–13]. The complete reduction sequences, including intermediate vertex names and dot positions, are in `support/geometry/movie_manifest.txt`; the accompanying rotation data fix their facial supports.

For example, the common undotted source underlying C_{14}, C_{19} reduces by the successive faces

$$(2,12,10,21),\ (3,4,14),\ (5,6,16,21),\ (7,15,17),\ (8,9,19,21),\ (11,20),$$

followed by the theta on vertices $13, 18$. The three squares use the pairings $(01)(23), (01)(23), (03)(12)$ in the displayed cyclic orders. The cap underlying B_{33} uses

$$(2, 10, 12),\ (9, 11, 19),\ (3, 4, 14, 20),\ (5, 6, 16),\ (7, 8, 18, 22),\ (13, 21),$$

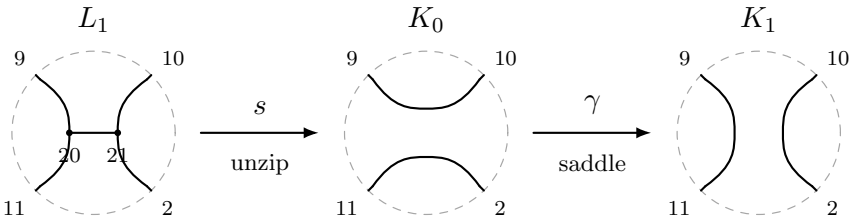
and then the theta on $15, 17$; its two squares use $(03)(12)$. The dot on C_{14} is on terminal theta edge 1, and that on C_{19} is on the selected bigon facet. The two dots on B_{33} lie on its selected bigon facet and terminal theta edge 0.

The *reference closure*, denoted Σ_{raw}, for a source P and cap R is

$$P\ ;\ s\ ;\ \gamma\ ;\ R. \tag{6.2}$$

Here s is the standard planar unzip, and γ the standard planar saddle between the adjacent matchings. The literal composite ba is not used in this definition.

Figure 8 shows the local slices of this planar middle. The cap at its right end is read in the direction displayed in Figures 5 and 6; a source at its left end is read in the reverse direction, as in Figure 4. For the two summands in the test for α, the corresponding reference closures use $P = C_{14}, C_{19}$ and $R = \mathrm{cap}(B_{33})$. This picture specifies the reference foam whose topology is computed below. The cobordisms and metric families defining h require the subsequent relative comparisons; the picture does not identify h with the composite γs.



The exterior E is carried along by the product.

Figure 8: The local slices of the planar middle in $\Sigma_{\mathrm{raw}} = P\,;\, s\,;\, \gamma\,;\, R$. The labels give the four attachment vertices in the common exterior. The first cobordism unzips the edge joining vertices $20, 21$; the second is the ordinary saddle between the two adjacent matchings.

Proposition 6.2 (Index of the reference closure)**.** *Every source–cap pair used in the three scalar tests has a reference closure with $Q = 5/2$ and $\nu = 0$. Its framed closure has $\chi(X) + \sigma(X) = 0$.*

Proof. Construct each facial move in $S^2 \times I$, using disjoint time intervals and the fixed product collars. The induced child rotation is precisely the rotation obtained by the prescribed local replacement. Thus the construction continues inductively through the reduction sequence. Cap its terminal theta by the standard three disks meeting along an interval in a ball. The source, the planar middle of (6.2), and the cap consequently lie in $S^2 \times I$ with a three-ball at each end, an oriented S^3. Lemma 6.1 gives $\nu = 0$. This argument places the whole foam in one three-manifold; planarity of its individual slices alone would not give the required normal section.

A local bigon or triangle reduction contributes zero to the Euler characteristic of a half-foam relative to its outgoing web; a square contributes -1. Indeed the local foam has Euler characteristic 1, whereas the outgoing local web has characteristic $1, 1, 2$, respectively. The half-theta has characteristic 1. A triangle contributes one tetrahedral point, and the other moves contribute none. Hence

$$\chi(P) = 1 - \#\{\text{squares in } P\}, \qquad \tau(P) = \#\{\text{triangles in } P\}. \tag{6.3}$$

The finite list reduces to the following table. Branch numbers here are zero-based; basis subscripts remain one-based.

Web	branches	squares	triangles	χ	τ
C	$0,1,4,5$	3	2	-2	2
C	$2,3$	2	4	-1	4
B	0	1	5	0	5
B	$1,2$	2	3	-1	3

One has $\chi(C) = -10$, $\chi(A) = \chi(B) = -9$. The global s and γ foams each have characteristic -10. Subtracting the three gluing webs therefore gives

$$\chi(\Sigma_{\mathrm{raw}}) = \chi(P) + \chi(R) + 8, \qquad \tau(\Sigma_{\mathrm{raw}}) = \tau(P) + \tau(R).$$

Each C row has $\chi - \tau/2 = -3$, and each B row has $\chi - \tau/2 = -5/2$. Thus $Q = -3 - 5/2 + 8 = 5/2$ for all eighteen possible branch pairs, including all the required pairs.

The underlying framed scalar is a cobordism from the empty Hopf object to itself. Joining its ordinary ends adds the time-circle handle to the closed S^4 picture, giving $S^4\#(S^1 \times S^3)$, with characteristic and signature zero. The marking Hopf annuli close to product tori; their Euler and normal numbers are zero. They do not change Q. □

The supporting calculation checks that each prescribed reduction takes place in a face of the planar web obtained at that stage. This verifies that the entire sequence can be realized as just described. The reason that the normal number is zero is the geometric one in the proof: the whole foam lies in an oriented three-manifold, and the resulting section of the squared normal bundle extends the prescribed seam section.

6.3 Comparing the augmented cobordisms

The scalar formula uses cobordisms obtained from the all-L triangle by the inclusions and projections in the local reduction formulas. We must compare these augmented cobordisms with the standard maps used above. The crossing and the position of the added edge are part of the comparison: they determine a normal number. We therefore specify the change from the pictures in [KM2] to our four labelled boundary points before making the index calculation.

To compare the all-L construction with the standard mixed triangle, fix the printed introduction/Section 8 convention of [KM2]. Its four ports are NW, NE, SE, SW; K_0 pairs horizontally, K_1 vertically, and K_2 joins NW to SE underneath the other diagonal. Identify these ports with $(9, 10, 2, 11)$ only after the following cyclic transport. Set

$$v_{NW} = (1,1,1), \quad v_{NE} = (1,-1,-1), \quad v_{SE} = (-1,1,-1), \quad v_{SW} = (-1,-1,1).$$

The screen coordinates $(X, Y, Z) = (-z, x, -y)$ have determinant $+1$. The NW–SE segment has depth -1, and the NE–SW segment has depth $+1$. Thus they realize the stated crossing, with positive depth towards the viewer. The rotation

$$R(x,y,z) = (y,z,x), \qquad \rho = (NE\ SW\ SE),$$

fixes NW, preserves orientation, and fixes time. It transports the printed (K_2, K_1, K_0) to the actual (K_0, K_2, K_1). The printed top augmentation edge travels to the left edge between ports $9, 11$. The entire local comparison, including its collars and edge strip, is transported. No symmetry of the exterior web is required.

Write

$$Q_H = P_{X,A}\widehat{H}I_Z, \qquad Q_F = P_{Y,W}\widehat{F}I_{X,A}.$$

These symbols in this subsection denote the actual composite foams.

Proposition 6.3 (Three relative replacements)**.** *For the standard embedded models with the transported collars just specified, the following relative differences hold:*

replacement	$\Delta\chi$	$\Delta\nu$	$\Delta\tau$
$ba-\gamma$	-1	2	0
$Q_H - s$	1	0	2
$Q_F - a$	1	-1	1

(6.4)

Each preserves Q.

Proof. The proof of [KM2, Theorem 9.1] identifies the literal ba with the saddle γ summed in a facet with Ψ_0. Since $(\chi,\nu,\tau)(\Psi_0) = (1,2,0)$ and a facet sum subtracts two from Euler characteristic, this gives the first row.

For Q_H, name the source vertices $20, 21$ as above. The triangle inclusion expands 20 to $(22, 20, 23)$, with the augmentation edge $(22, 23)$. After $\widehat{H}$, the upper and lower square paths are $9, 22, 24, 10$ and $11, 23, 25, 2$, with vertical edges $(22, 23), (24, 25)$. The A projection pairs 22 with 24, and 23 with 25. The two tetrahedra are joined by the three seam paths through 20, through $22, 24$, and through $23, 25$. The intervening facets are the standard untwisted disks. This is the collapsed-side triangle comparison on a theta boundary: its two fillings have characteristics $2, 1$ and numbers of tetrahedra $2, 0$. Both lie in the same local three-dimensional host, with the same collar framing, so their normal difference is zero. This proves the second row. This theta boundary must be distinguished from the prism boundary for an inverse on the triangle side.

For the last row, use the embedded identity in the *proof* of [KM2, Lemma 8.2], followed by its complete Figure 9 movie. The middle band in that movie is the standard tetrahedral cobordism summed with positive Ψ_2. The surrounding square inclusion and projection give

$$Q_F \#_{\text{tet}} \Psi_2 \cong a \#_{\text{facet}} \Psi. \tag{6.5}$$

The source identifies the capping disk with D_+ of its Proposition 4.7. The identity therefore specifies both the foam and the facet; equality of the resulting homology maps would not be sufficient.

From the definition $\Psi_n = \mathbb{RP}^2 \cup D_1 \cup \cdots \cup D_n$ in [KM2, Section 4], one obtains $\chi(\Psi_n) = 1+n$, $\nu(\Psi_n) = 2-n/2$, and $\tau(\Psi_n) = n(n-1)/2$. In particular positive Ψ_2 has tuple $(3, 1, 1)$. In a standard tetrahedral sum the two removed cones each have characteristic 1, and their common link K_4 has characteristic -2. The glued characteristic is therefore the sum minus four, and the two tetrahedral points disappear. The in-three-plane normal lines on the removed facet sectors match under the specified cone-link gluing, so ν adds. Inserting Ψ_2 changes the tuple by $(-1, 1, -1)$. The source's description of Ψ as $\overline{\Psi}_2 \#_{\text{tet}} \Psi_2$ gives its tuple $(2, 0, 0)$, so a facet sum with Ψ changes none of the three numbers. Solving (6.5) now gives $\Delta(Q_F - a) = (1, -1, 1)$. The normal sign is determined by this equation. The external reflected cap is attached to both sides with the same collar; it does not introduce a second reflection. The final assertion follows by substitution in (6.1). □

For the representative source and cap used to compute α, the reference foam has $(\chi,\nu,\tau) = (5, 0, 5)$. The three replacements give successively

$$(5, 0, 5) \longmapsto (4, 2, 5) \longmapsto (5, 2, 7) \longmapsto (6, 1, 8).$$

There is a separate Euler check on the actual seven-piece augmented movie: its pieces have characteristics $-2, -10, -11, -11, -10, -10, -1$, while the six intermediate webs have characteristics $-10, -11, -11, -11, -9, -9$. Thus $\chi = -55 + 61 = 6$; the tetrahedral counts sum to eight. The augmented foam need not lie in the three-sphere containing the reference foam. Its normal number is supplied by Proposition 6.3.

6.4 Excision and the retained empty factors

The construction in Section 4 replaces a local foam relation by a sum of one-parameter families on larger cobordisms. We now check that the extra pieces introduced there do not change I_{top} after the source and cap have been attached. By the *excess* of a piece we mean its contribution to the difference between this closed index and the index of the corresponding original cobordism. The comparison uses the punctures, framed arcs, product spectator tubes and Hopf core specified in Proposition 4.2. An arbitrary inverse of the excision map on homology would not determine these data.

Keep the actual empty Hopf complex U in the geometry, even when it is suppressed from formulas for maps. The reference comparison is with $F_j \otimes 1_U$. Its closed U product adds $S^1 \times S^3$ with two Hopf tori, and has zero ambient and singular contribution to (6.1).

The standard four-ended Hopf core W_H has relative handles of indices $1, 2, 2, 3$. Its Kirby description gives

$$W_H \cong (I \times S^3)\#(I \times S^3)\#(S^2 \times S^2), \qquad \chi(W_H) = \sigma(W_H) = 0;$$

see [ISST, Section 4, Lemma 4.1 and Figures 6–8]. For completeness, the zero normal contribution concerns the *total* four annuli. Label them (i, ε) for $i = 1, 2$, $\varepsilon = +, -$. The nonzero incoming linking entries pair equal i and unequal ε; the outgoing entries pair unequal i and equal ε. Each entry is $+1$, and both ordered sums are four. Their difference, the relative normal contribution, is zero. The reversed block has the same zero excess. This uses the fixed boundary framings, not merely the fact that the sheets are annuli.

A product spectator $K \times I$ has characteristic $\chi(K)$, which must be retained. If P_j is a filling of Q and O its common exterior, then for spectator K

$$\chi(L_j) = \chi(K) + \chi(P_j), \qquad \chi(\Psi_{\mathrm{spectator}}) = \chi(K) + \chi(Q).$$

Subtracting the intermediate web in either side of the naturality comparison leaves $\chi(K) + \chi(P_j)$. Attaching O gives

$$\chi(P_j) + \chi(O) - \chi(Q) = \chi(F_j). \tag{6.6}$$

Thus the spectator has zero *relative excess*. The same product collars identify the normal sections, and introduce no tetrahedra.

The local relative invariant punctures a four-ball away from the foam, changing its ambient characteristic from one to zero. The equivalent boundary-connected insertion has a four-ball and a joining one-handle, also with net ambient contribution zero. No unpaired zero-handle is lost in passing between these descriptions.

The inverse comparison uses the torus cut of [KM4, proof of Theorem 5.6, Figure 5]. Its removed $T^3 \times I$ and the two inserted $T^2 \times D^2$ have characteristic and signature zero and are disjoint from the foam. The cuts are closed internal three-manifolds, so ordinary signature additivity applies without a corner correction. Consequently composition comparison, either torus stretching comparison, and product continuation have zero excess. The matching-orbit identification of Section 4.3 uses these same pieces with the same product bundle and cap framings. It changes neither the topology nor

the action of a matched configuration; the torus-only reference factors are flat. With the notation of the localization construction, every term

$$R_j, \quad ON_jV', \quad OL_jH_{\mathrm{comp}}, \quad OL_jH_{\mathrm{cut},c}, \quad OL_jH_{\mathrm{cut},p}, \quad OL_jH_{\mathrm{cont}}$$

has the same closed I_{top} as the corresponding capped F_j. This is a calculation for sums of one-parameter families. Two varying families are never multiplied together.

6.5 The index of every term in the scalar expressions

It remains to combine these comparisons for the finite sum in Proposition 5.2. There are two points to check: the successive local reductions must preserve the topological term in the closed index, and each term must still have just one family parameter. The second point follows from the form of the sum: its homotopies are added, and each composite contains only one varying factor.

Proposition 6.4 (Index of the specified expansion)**.** *For the localization families on the specified geometries, every constituent of the capped three-scalar expression has $\chi(X)+\sigma(X) = 0$ and $Q = 5/2$. Each has one family parameter. It has three dots for α, β and two dots for either fixed cap summand of χ.*

Proof. The two changes $ba - \gamma$ and $Q_F - a$ have sum $(0, 1, 1)$. A previous triangle collapse followed by its reverse expansion adds $(1, 0, 2)$; a square inclusion/projection branch has the same relative triple as the square cylinder. For a triangle-side inverse the local boundary is L_3, of characteristic -3. Its product filling has $(\chi, \nu, \tau) = (0, 0, 0)$ and its collapse/expansion filling has $(1, 0, 2)$. In (6.6), one must subtract this prism boundary, not a theta boundary. The difference of the two resulting closed triples is still $(1, 0, 2)$.

It follows that the change from the reference closure to any term in the scalar expression is

$$(\Delta\chi, \Delta\nu, \Delta\tau) = (n, 1, 2n + 1), \tag{6.7}$$

where the actual position of the local filling determines n:

Constituent	n
Main $\widehat{J}$, T_X, or $L_{H,B}$	1
$L_{H,A}$, the Q_H filling	1
$L_{H,A}$, the s filling	0
A square term of T_A	0
Triangle term at position j, product filling	$j - 1$
Triangle term at position j, collapse/expansion filling	j

For the last two rows, $j - 1$ counts the preceding paired triangle collapses and expansions. The channel lengths are $2, 4, 4, 3$, so $0 \le n \le 4$. All terms in the local construction retain the value for their chosen filling by the zero-excess calculation above. Finally,

$$\Delta Q = n + \tfrac{1}{2} - \tfrac{1}{2}(2n + 1) = 0.$$

Proposition 6.2 supplies the baseline. Every homotopy is a sum of one-parameter constituents, and all surrounding maps have zero parameters. The source has one dot, B_{33} has two, and B_2, B_7 have one each; none of the constructions adds dots. □

The supporting term catalogue checks the sources and targets in every composite and assigns (6.7) to each filling slot. It verifies completeness and arithmetic, but assumes the geometric identifications proved or specified above. Its entries do not constitute independent evidence for an embedded isotopy or a normal framing.

There is a final distinction concerning closure. A closed count equals an algebraic trace only with the appropriate class dual to the glued hypersurface included in the finite gauge subgroup; [KM4, Proposition 5.5 and its following remark] explains the possible extra factor of two. We do not use a trace-count equality. Instead, a matched broken configuration provides bundle identifications at its nondegenerate ends. Splicing those data and closing the retained empty factors gives closed bundle data to which the additive index formula applies. The spliced connection need not be anti-self-dual. Finite gauge covers do not change its Chern–Weil action or local Fredholm index; the Hopf restriction has zero stabilizer Lie algebra.

Thus, subject to the realization and regularity statements, a contribution to a zero-dimensional, k-dotted, one-parameter constituent must satisfy

$$0 = 8\kappa + \tfrac{5}{2} - k + 1, \qquad \kappa = \begin{cases} -1/16, & k = 3, \\ -3/16, & k = 2. \end{cases} \tag{6.8}$$

This is an index requirement on the specified contributions, not yet an assertion that they vanish. The uniform energy estimate is the additional analytic input needed for that conclusion.

7 Perturbations and the action estimate

An unperturbed anti-self-dual connection has nonnegative action. For a perturbed equation the action may be negative, but its negative part can be bounded in terms of the perturbation. We first prove a bound that is uniform as the necks in our cobordisms become long. The important point is to use the gradient-flow identity on a cylindrical region; estimating the perturbation there by its four-dimensional L^2 norm alone would introduce an unwanted factor of the neck length.

We must then choose perturbations that satisfy this bound and make all the required moduli spaces regular. They must agree whenever two families have a common boundary face, and they must preserve the chosen local Floer complexes. The torus ends require the correlated marking data of Section 4.3. The construction of these simultaneous choices occupies the rest of the section and is assembled in Theorem 7.8.

7.1 A uniform estimate on stretched pieces

We use the action normalization of [KM1, Proposition 2.6]. On a compact four-dimensional piece Q, with the orbifold integral and the corresponding invariant inner product on $\mathfrak{so}(3)$, the Chern–Weil identity is

$$\kappa_Q(A) = \frac{1}{32\pi^2}\big(\|F_A^-\|^2_{L^2(Q)} - \|F_A^+\|^2_{L^2(Q)}\big). \tag{7.1}$$

Consequently, a solution of $F_A^+ = q(A)$ satisfies

$$\kappa_Q(A) \geq -\frac{1}{32\pi^2}\|q(A)\|^2_{L^2(Q)}. \tag{7.2}$$

The sign convention for q is immaterial to this inequality.

Applying (7.2) to an entire long cylinder would give an unhelpful bound proportional to its length. The gradient structure gives a better estimate. Normalize a lift $\mathcal{C}$ of the Chern–Simons

functional and the metric on configuration space so that its drop is the action on a cylinder and its negative gradient equation is the unperturbed ASD equation. A lift along a particular path suffices; no globally real-valued lift of $\mathcal{C}$ is asserted. Perturbations f_t, in contrast, are globally defined bounded gauge-invariant real-valued functions.

Lemma 7.1 (Neck estimate)**.** *Suppose $a(t)$ satisfies*

$$\frac{da}{dt} = -\operatorname{grad}(\mathcal{C} + f_t)(a(t)), \qquad t \in [t_-, t_+].$$

Then

$$\kappa_{[t_-,t_+]}(a) = \int_{t_-}^{t_+} \left\| \frac{da}{dt} \right\|^2 dt + f_{t_+}(a(t_+)) - f_{t_-}(a(t_-)) - \int_{t_-}^{t_+} (\partial_t f_t)(a(t))\, dt, \tag{7.3}$$

$$\kappa_{[t_-,t_+]}(a) \geq -\|f_{t_-}\|_\infty - \|f_{t_+}\|_\infty - \int_{t_-}^{t_+} \|\partial_t f_t\|_\infty\, dt. \tag{7.4}$$

For a constant $f_t = f$, the last bound improves to $-\operatorname{osc}(f)$.

Proof. The chain rule gives

$$\frac{d}{dt}(\mathcal{C}(a(t)) + f_t(a(t))) = -\left\| \frac{da}{dt} \right\|^2 + (\partial_t f_t)(a(t)).$$

Integration and the identification of the drop of $\mathcal{C}$ with the Chern–Weil integral give (7.3). Dropping the nonnegative integral gives both inequalities. The calculation retains the chosen path lift, including its action period. It makes no use of regularity or nondegeneracy. □

Call a decomposition of a family into cylindrical regions and complementary compact cores *controlled* if its necks carry equations of this gradient form and if there are constants $\eta, \epsilon \geq 0$ such that

$$\sum_{\text{necks } j} \left(\|f_{j,t_-}\|_\infty + \|f_{j,t_+}\|_\infty + \int \|\partial_t f_{j,t}\|_\infty\, dt \right) \leq \eta, \tag{7.5}$$

$$\sum_{\text{cores } Q} \|q_Q(A)\|^2_{L^2(Q)} \leq \epsilon. \tag{7.6}$$

These bounds are required for every configuration in the relevant bundle sectors and uniformly in the metric-family parameter, including arbitrary neck lengths. The first expression may be replaced by its sharper telescoped version when adjacent necks have the same end perturbation.

Proposition 7.2 (Uniform action bound)**.** *Every solution for controlled data satisfies*

$$\kappa_{\text{total}} \geq -\eta - \frac{\epsilon}{32\pi^2}. \tag{7.7}$$

The same conclusion holds for endpoint-matched broken configurations if the data on the matched ends agree and the displayed bounds apply to the underlying finite collection of cobordism pieces.

Proof. The Chern–Weil integral is additive on the decomposition. Sum (7.2) over the cores and (7.4) over the necks. For infinite ends, first truncate and then pass to the limit using convergence to the prescribed critical points.

For a broken configuration the same argument applies to its pieces. At an inserted Floer breaking, the endpoint values of f in (7.3) cancel, because the critical point and perturbation are the same on the two sides. The nonnegative gradient energies add. Thus subdividing a cylindrical trajectory into several levels does not increase the perturbation error in the lower bound for action. This cancellation is preferable to assigning a separate oscillation bound to each level. The other compact pieces and cutoff regions belong to the fixed finite construction and retain their original bounds. This proves the assertion also for broken products. □

The required uniformity can be checked before making any regularity claim. For example, put $f_t = \vartheta_t f$ on a neck, where ϑ_t is constant on its long middle interval and has transitions in collars of fixed width. Then

$$\int \|\partial_t f_t\|_\infty \, dt \le \mathrm{TV}(\vartheta)\|f\|_\infty.$$

The right-hand side does not depend on the length of the middle interval. On a compact family of core metrics, a uniformly bounded holonomy perturbation of size $O(\lambda)$ has squared L^2 norm $O(\lambda^2)$. For finitely many such pieces, the total error in the action bound is therefore $O(\lambda) + O(\lambda^2)$. This is an estimate on the admissible space of perturbations. Scaling a particular regular perturbation need not preserve regularity; regular data must be chosen inside the resulting small open set.

7.2 Transversality with the endpoint complexes fixed

The perfect local complexes of Section 3 were obtained by particular choices of perturbation. Those choices must remain fixed on the infinite ends of each cobordism. There is nevertheless freedom to perturb the equation on a finite cylindrical region inside the cobordism. We use this freedom for transversality.

Fix a good endpoint functional $\mathcal{C} + f_\pi$, using the local and terminal models of Proposition 3.1 where required. This fixes the critical points and the trajectory differential. On a finite product subcollar $J \times Y$, add a time-dependent perturbation of the form

$$h(t, a) = \sum_{i,j} c_{ij} \chi_i(t) f_j(a).$$

Here f_j are marked cylinder functions separating tangent vectors of the configuration quotient, and the χ_i are dense among smooth time bumps supported in J. We call h a secondary perturbation, to distinguish it from the perturbation already fixed on the end. It is zero outside a finite cylindrical region. Within that region it need not vanish near configurations that represent endpoint critical points. Thus even a solution that is constant on this region can be tested by all the cylinder-function directions, without changing the Floer complex on the end.

Choose a weighted ℓ^1 norm $\sum C_{ij}|c_{ij}|$, with weights dominating the tame cylinder-function estimates and the time derivatives. As in the usual diagonal construction of the perturbation space, the weights can control every prescribed derivative order. In particular the norm controls

$$\sup_t \|h_t\|_\infty + \int_J \|\partial_t h_t\|_\infty \, dt + \sup_{t,a} \|\operatorname{grad} h_t(a)\|_\infty. \tag{7.8}$$

Every individual time bump times a cylinder function belongs to this separable Banach space. Multiplying by parameter bumps gives the relative family version. The marked cylinder functions are those of [KM1, Section 3.2]; their analytic estimates have the bounded-operator form of [KM5, Propositions 3.7 and 3.15].

Proposition 7.3 (Ordinary collar surjectivity)**.** *Let X be a completed bifold cobordism with fixed nondegenerate asymptotic data. Suppose:*

1. *every connected component has an ordinary strongly marked end with a finite product subcollar admitting the secondaries above;*
2. *every nonlocal equation perturbation is a time-dependent gradient perturbation on a product cylindrical region; the complementary cores are unperturbed;*
3. *each finite gauge quotient used on a component has zero restriction in the marking quotient at its chosen ordinary end.*

Then the universal connection-and-secondary linearization is surjective at every solution. The assertion holds with the endpoint complexes fixed, in arbitrarily small open balls of secondary perturbations, and at interior parameter points using variations vanishing on previously fixed parameter-boundary collars.

Proof. Write the equation as $F_A^+ + q(A) = 0$ and its linearization as $L_A = d_A^+ + Dq_A$. On the usual unweighted Sobolev completions the nondegenerate ends make the gauge-fixed operator $D_A = (d_A^*, L_A)$ Fredholm. Let (ϕ, η) annihilate both its range and every secondary direction. Thus

$$d_A\phi + L_A^*\eta = 0.$$

Gauge covariance at a solution gives $L_A d_A = 0$. Testing against compactly supported $d_A\xi$ yields $\Delta_A\phi = 0$. Cutoff integration by parts on the cylindrical ends gives $d_A\phi = 0$. A nonzero parallel section cannot be L^2 on an infinite end. Hence $\phi = 0$, and the remaining equation is

$$L_A^*\eta = 0. \tag{7.9}$$

In temporal gauge on the control collar, write $\eta = dt \wedge \zeta + *_Y\zeta$. The perturbation has no dependence on the temporal component of A. The temporal component of (7.9) therefore says $d_a^*\zeta = 0$. Orthogonality to the variation $\chi_i(t)f_j(a)$ says

$$\int_J \chi_i(t)\, df_j|_{a(t)}[\zeta(t)]\, dt = 0.$$

Time localization implies that every df_j annihilates $\zeta(t)$ at each t. Since ζ is horizontal and marked cylinder functions separate tangent vectors, $\zeta = 0$ on the entire subcollar.

On an unperturbed core, elliptic unique continuation propagates this vanishing. On a nonlocal product collar use Lemma 7.4 below, rather than local unique continuation for a nonlocal equation. Alternating these two arguments reaches the entire connected regular part of X; orbifold smoothness extends the conclusion across its singular set. Thus $\eta = 0$ everywhere. The connection operator is Fredholm, so adding the secondary directions to its range gives a closed subspace of finite codimension. Its annihilator is zero, which proves surjectivity.

At an interior parameter point, multiply the secondary variation by a parameter bump equal to one there and zero on the fixed boundary collars. This proves the relative interior assertion.

The quotient restriction in the statement means restriction is zero in the *marked gauge quotient*, not merely that the quotient preserves the endpoint critical set. All control-collar cylinder functions are therefore already invariant. There is no averaging loss of directions. If a quotient element fixes a connection class, its representative, after composition with an allowed gauge transformation, is parallel. At the strong end it is a marked automorphism and hence the identity; parallel uniqueness gives the identity on the component. The effective finite quotient acts freely, and the upstairs surjectivity descends. □

Lemma 7.4 (Temporal continuation across a nonlocal collar)**.** *Suppose a smooth Hilbert-space-valued section satisfies $u' = B(t)u$, where $B(t)$ is self-adjoint on a common first-order Sobolev domain and $B'(t)$ is bounded on L^2 on compact time intervals. If u vanishes on a nonempty time interval, it vanishes throughout the connected interval of definition.*

Proof. Where $h(t) = \|u(t)\|^2 > 0$, differentiation gives

$$h' = 2\langle Bu, u\rangle, \qquad h'' = 2\langle B'u, u\rangle + 4\|Bu\|^2,$$

and consequently

$$(\log h)'' \geq -2\|B'\|.$$

If $\|B'\| \leq C$, the function $\log h + Ct^2$ is convex. Its supporting tangent line at an interior point is a finite lower bound at a finite endpoint. Thus h cannot tend to zero at such an endpoint of a positivity interval. This proves the assertion in both time directions. □

For the adjoint equation above, put $u = (0, \zeta)$ in $\Omega^0(Y; \operatorname{ad} E) \oplus \Omega^1(Y; \operatorname{ad} E)$. The temporal constraint and spatial equation give such an evolution, with extended Hessian, up to the fixed sign convention,

$$B(t) = \begin{pmatrix} 0 & d_a^* \\ d_a & *_Y d_a + \operatorname{Hess}_a f_t \end{pmatrix}.$$

The product metric is independent of physical time. Differentiating d_a contributes multiplication by $a'(t)$; differentiating the perturbation Hessian gives a bounded L^2 operator, smoothly in t. This verifies the hypotheses of the lemma. In particular, the proof does not apply local unique continuation across a spatially nonlocal holonomy term.

7.2.1 Relative regularity and ideal configurations

Sard–Smale gives regular secondary perturbations inside any sufficiently small open ball of the permitted perturbation space. This is how we obtain smallness and regularity at the same time; scaling a perturbation after making it regular would not justify the assertion. The condition that the endpoint differential vanish imposes no additional restriction on these perturbations supported in finite collars. A uniform spectral gap as the endpoint perturbation tends to zero is also unnecessary: choose the endpoint perturbation first, then use its fixed positive gap.

Relative boundary regularity still comes from the actual gluing theorem. Surjectivity in a parameter interior cannot identify a torus-cut face or prescribe its gauge quotient. These are addressed separately below. All nonlocal perturbations can be kept on product collars, including the collars inherited at a glued face. The compact cores can carry the unperturbed ASD equation.

The freeness argument also applies to an ideal background retaining the ordinary strong end. A sufficiently small neighborhood of that background is disjoint from its nontrivial finite translates. Therefore the quotient does not identify different branches over that same ideal background. The four local tetrahedral bubble branches of [KM1, Proposition 2.9 and Section 3.4] retain their even multiplicity. This argument is local to an open piece with a strong end; it asserts nothing about a closed quotient without such an end.

7.3 Compactification and gluing at the torus ends

In the excision comparison, stretching the internal torus separates an exterior cobordism from a cylinder or from two copies of $T^2 \times D^2$. We need to know that only the flat connections on these

torus pieces can occur at the ends of the zero- and one-dimensional moduli spaces. We must also check the gluing multiplicity, retaining the two boundary lifts together as in Section 4.3.

Keep the torus necks and caps unperturbed. Choose the secondary perturbations on finite collars at the ordinary ends of the exterior, and put all dots on the exterior factors. Proposition 7.3 then makes the exterior regular in every relevant relative bundle class, with data invariant under the finite action used in Lemma 4.1. The next lemma provides the index gap that excludes nonflat torus pieces.

Lemma 7.5 (Flat cap inverse and index gap)**.** *Choose the cap metric as a flat T^2 times a disk completed with a cylindrical end, with the product flat bundle fixed in Section 4.3. Its flat ASD deformation operator is invertible and has index zero. Every nonflat finite-energy unperturbed ASD cap has index at least four. Every nonconstant unperturbed ASD torus level has parameterized index at least four.*

Proof. Each of the three real characters in the adjoint local system is nontrivial on a circle of T^2. The twisted torus Laplacian therefore has a positive lower bound in every form degree. The product Laplacian on the completed cap retains that bound. At a flat connection the scaled ASD operator

$$D = d_A^* \oplus \sqrt{2}\, d_A^+$$

has D^*D equal to the twisted Hodge Laplacian on one-forms and DD^* equal to its counterpart on zero-forms and self-dual two-forms. The spectral bound gives a bounded inverse. This proves both kernel and cokernel vanish, not just the vanishing of ordinary cohomology. The same reasoning applies to the flat cylinder.

For the finite stabilizer, the three nonidentity elements of the V_4 centralizer have lift obstructions dx, dy, and $dx + dy$. They are excluded by the determinant-one marking, including its extension by the angular class ds alone. The latter exchanges the two lifts and does not stabilize either. Thus no discrete stabilizer factor has been concealed in the acyclicity statement.

Compare a cap solution with the oppositely oriented flat reference. The double has underlying manifold $T^2 \times S^2$. Writing x, y for its two degree-two generators, its bundle has $w_2 = x + \varepsilon y$, where $\varepsilon \in \{0, 1\}$ records the possible boundary lift. The Pontryagin square evaluates to 2ε mod 4, so the relative action belongs to $\frac{1}{2}\mathbb{Z}$. The boundary adjoint operators of the two lifts are conjugate; their spectral corrections agree. Relative to the index-zero flat cap, the index is 8κ. Unperturbed ASD gives $\kappa \geq 0$, with equality only for a flat connection. Thus a nonflat cap has $\kappa \geq \frac{1}{2}$ and index at least four.

For a cylinder level, the corresponding mapping-torus comparison is on T^4. The fixed T^2 class plus a class $\lambda \smile [dt]$ again has even Pontryagin square, giving half-integral action. Its relative index is 8κ, with equal adjoint spectral corrections at the two ends. A nonconstant ASD level has positive action, proving the same bound. Equivalently, the angular lift exchange has spectral-flow shift four. □

Proposition 7.6 (Torus compactification and gluing)**.** *For the composite and product torus-stretching families of Section 4.3, the torus ends of the zero- and one-dimensional cut-down moduli spaces consist exactly of the regular matching exterior configurations glued to the flat cylinder or to the two flat caps. Both ends count $Q_{\mathfrak{a}}$ with multiplicity one. The assertion is relative to the fixed ordinary boundary data and is compatible with ordinary Floer breaking.*

Proof. First exclude extra torus pieces. Fredholm indices add across the acyclic torus ends. All cut-down constraints are on the exterior Z_{cut}. Let $D \leq 1$ be the total cut-down family dimension, let $r \geq 1$ be the codimension of the parameter face, and let p_∂ be its dimension. If m is the cut-down

degree, j_h the cap indices and d_ℓ the parameterized indices of genuine torus levels, the exterior family has expected dimension

$$e_{\mathrm{ext}} = d_{Z_{\mathrm{cut}}} + p_\partial - m = D - r - \sum_h j_h - \sum_\ell d_\ell. \tag{7.10}$$

There is no continuous torus matching space to subtract. A constant flat cylinder is matching data and has no translation dimension to subtract; a genuine nonconstant level contributes its parameterized index in this formula. Any nonflat cap or nonconstant torus level would make e_{ext} negative. The corresponding exterior moduli space is empty by its independently achieved regularity. For a disconnected exterior this means regularity of the joint family, using independent collar directions on its components and counting a shared parameter only once. At a torus breaking without a parameter degeneration the same argument uses $r = 0$. Additional ordinary breakings only reduce the dimension available. Smooth bubbles on the torus-only pieces also force a negative-index exterior. No regularity assertion for high-index unperturbed cap or torus moduli is needed here.

For a surviving flat broken configuration, the torus Hessian is invertible with a fixed spectral gap. The exterior solution has exponentially decaying tails. Choose a bounded right inverse to the regular exterior operator on the complement of its finite-dimensional kernel, including the linearized dot constraints. The flat local piece has the inverse in Lemma 7.5.

Splice the solutions and their inverses along necks of length R. The equation error decays exponentially. The linear parametrix error is the sum of exponentially small tail errors and cutoff commutators. Allowing the *parametrix* cutoff transitions to grow with R makes the latter $O(R^{-1})$. These cutoffs are used only in solving the linear equation; they do not lengthen any physical secondary perturbation support. The absence of a torus zero mode prevents a new small cokernel mode: a normalized approximate cokernel section would limit either to a cokernel section on an exterior or cap, or escape down the neck, where the spectral gap excludes it. Thus the right-inverse estimate is uniform after the exterior kernel is split off. For large R the parametrix error has norm less than one. A Neumann series gives a right inverse, and the quadratic remainder estimate gives the unique nearby solution modulo gauge by contraction mapping. The exterior kernel and the neck length are the chart parameters.

These estimates are uniform on compact subsets of the regular broken stratum. Uhlenbeck compactness and exponential convergence give the converse: a sequence tending to the torus end approaches one of these flat broken configurations, since the index argument has excluded other torus or cap factors. Hence the gluing charts describe the full end under consideration.

For the product family, there are two cap boundaries but only one chosen stretching parameter. First allow independent lengths (R_1, R_2). Acyclic gluing gives the local chart

$$\mathcal{M}_{\mathrm{ext}} \times [R_0, \infty)^2,$$

with submersive projection to the lengths. Restricting to $R_1 = R_2$ gives the required chart $\mathcal{M}_{\mathrm{ext}} \times [R_0, \infty)$. Thus this joint degeneration has codimension one, not two; the diagonal restriction loses no regularity.

Construct the charts before the extra finite quotient. The matching orbits on the composite are $(\mathcal{X}_{00} \sqcup \mathcal{X}_{11})/G$, and the product selects $\mathcal{X}_{00}/G_0$. Lemma 4.1 identifies these charts and their counts once each. The tree and forest incidence graphs there account for all central-lift multiplicities.

At an ordinary breaking use the fixed good ordinary endpoint data. Splicing in disjoint cylindrical regions gives the ordinary gluing parameters together with these torus parameters. In the dimensions at issue an additional independent degeneration at a torus end has codimension at least two and gives no new endpoint. This refers to an additional breaking, not to the two prescribed cap lengths

sharing one parameter. Exterior tetrahedral bubbling retains the ordinary four-branch local model and its even count, by the free-quotient argument following Proposition 7.3. □

The underlying elliptic slice, Uhlenbeck compactness and cylindrical-end nonlinear estimates are those of the bifold construction in [KM1, Section 3.4] and the broken-metric family framework in [KM4, Section 3.9]. The arguments above verify the additional restricted perturbation directions, torus-only inverses, index gap, diagonal length restriction and finite multiplicities needed for these particular families.

7.4 Compatible choices with a uniform action bound

We have established transversality for the permitted perturbations and described gluing at the torus ends. We now choose the data for all the cobordisms and families in Section 4 at once. The choices are made in an order that fixes each boundary face before the interior of a family is treated. Their smallness will give a uniform lower bound for the action of every configuration counted in the three scalar expressions.

7.4.1 Choose the local models in the normalization first

Begin with the families of metrics used in the all-L exact-triangle argument of [KM2]. These include the local sphere models and the permitted metric choices on the special face. Take their restrictions for the metrics on the ordinary all-L cobordisms. Thus we choose the map metrics as part of this family, rather than prescribing them in advance and seeking an extension.

Fix the complete local $S^{2,1}$ and sphere models at this stage, including their allowed generic metric families and their common corner data. Subsequently, the secondary perturbations for the counted all-L operations will be supported on collars at ordinary external ends, outside these local pieces. The local models can therefore be used with the metric freedom allowed in the published argument; no additional relative metric assertion for the special face is required.

For clarity, the compactified pentagon has successive boundary faces

$$Y_2, \quad S_1, \quad S^{2,1}, \quad S_2, \quad Y_1.$$

These are the disjoint-cut adjacencies, not the cyclic intersection order of the five hypersurfaces. The special face is adjacent to the two sphere faces. The construction and permitted local metric freedom are those of [KM2, Sections 6–7]. The two-parameter families used to prove the normalization do not occur in the scalar expressions. We need not impose the smallness bound for action on these auxiliary families, although their data must agree with the selected data on the counted boundary faces.

Choose each remaining collared geometry before its equation perturbations. A compact initial path from a prescribed metric to a neck-adapted metric can be included before stretching. It is still a one-parameter family on the same cobordism and changes neither its topological index nor the number of parameters.

7.4.2 A finite order of choices

The order below is useful because it leaves no equation requiring a choice to be invariant under its own subsequent compositions.

1. Choose the common endpoint data once for each labelled marked end. For a perfect local or terminal complex, choose the small model perturbation, then a good additional perturbation vanishing near its nondegenerate critical set.

2. Choose the ordinary maps, source and cap fillings, p_j, O, L_j, F_j, the excision maps, and the reduction maps. Repeated labels mean identical data.

3. Choose the common cut-open exterior with its correlated torus data, and finite reference composite and product cores.

4. Choose the interval families relative to their already chosen faces: composition, spectator translation, the two torus stretchings, product continuation, and the all-L J families.

5. Complete the all-L normalization relative to its selected faces, within the families of metrics in the published construction.

No interval interior is prescribed as another interval's endpoint. The localization construction uses an algebraic sum and composition of these homotopies. It does not assert that they are faces of a further unconstructed higher-dimensional family.

The local relation needs no further choice constraint. If $p_j : U \longrightarrow D$ are the relative maps into an actual perfect local complex, then $d_U = d_D = 0$. The homology relation $\sum_j [p_j] = 0$ implies the literal chain relation $\sum_j p_j = 0$. Interior changes of a filling map are chain homotopies and hence change none of its entries with these endpoints. This is why the p_j can be made regular and small independently.

For relative extension, use collared identifications to view the permitted perturbations as sections of the fixed Banach spaces. Pull back face data over parameter collars and extend with a partition of unity in parameter space. A parameter derivative is not a physical time derivative in the energy identity. Finitely many extension charts have a finite total norm loss. Choose successive generic corrections in smaller open balls, vanishing on already fixed parameter collars. Proposition 7.3 supplies interior surjectivity; ordinary marked gluing and Proposition 7.6 supply regularity at the fixed collars. The conditions for all relative bundle classes and endpoint labels form a countable collection, so their residual regularity sets can be intersected inside each small open ball.

Dot sections are chosen once on the ordinary factors and pulled back on matched faces. Their relative extensions can be made transverse separately. They change no equation perturbation and incur no action cost. Their associated line bundles and the boundary identifications must be retained; in this construction the dots lie on the ordinary source and cap pieces, where the ordinary marking is fixed.

7.4.3 The estimate on a whole capped constituent

Apply the exact neck identity (7.3) and the core bound (7.2). Fixed-width physical cutoffs give the length-independent total-variation bound above. Translating such a transition or lengthening the constant middle of a neck has the same bound. The cap and torus equations remain exactly unperturbed.

Let ρ bound the endpoint and secondary norms after the finite extension losses. There are constants C_1, C_2, fixed by the chosen geometric families and cutoff functions, so that each basic counted piece has a cylindrical contribution to the action error at most $C_1\rho$ and a squared perturbation norm on the compact core of at most $C_2\rho^2$. These are bounds on the whole configuration space in all relevant sectors, not estimates for a selected solution.

Let L bound the number of basic factors in a capped constituent. The list of composites specified in Appendix A contains at most 18 operators in any one term; adding source and cap permits $L = 20$, with fixed component multiplicities absorbed in the constants. Thus every constituent satisfies

$$\eta + \frac{\epsilon}{32\pi^2} \leq LC_1\rho + \frac{LC_2\rho^2}{32\pi^2}. \tag{7.11}$$

For a prescribed $\delta > 0$, choose ρ so both summands are less than $\delta/4$, leaving room for subsequent relative choices. Regularity is obtained inside that open set. No lower bound on perturbation size is imposed by the surjectivity argument.

At a Floer breaking, the two appearances of the same endpoint value of f in (7.3) cancel. Arbitrarily many trajectory levels therefore do not create arbitrarily many oscillation penalties. The same applies at ordinary matched ends of a composed word. There remain only the finitely many prescribed transition regions and compact cores. The bound persists on the broken faces.

The gluing threshold may grow as ρ decreases and the local spectral gaps shrink. Choose ρ and the endpoint data first; use their gluing threshold afterward. All the extra length is assigned to gradient cylinders, where (7.3) is independent of length, rather than to a volume estimate for an uncontrolled perturbation.

Proposition 7.7 (Coherent regular data with quantitative control)**.** *For the collared family geometries of Section 4, with the ordinary marked gluing and the torus identifications proved above, the fixed perfect endpoint complexes, ordinary regularity and agreement on common faces can be imposed simultaneously with an arbitrarily small uniform perturbation error in the action bound.*

Proof. Use the finite order above, relative affine extension, and residual regular choices in the open balls supplied by Proposition 7.3. Use the flat models of Lemma 7.5 on the isolated torus-only pieces and the published sphere and $S^{2,1}$ models on the normalization faces. Formula (7.11) applies to every word; the endpoint cancellation proves the assertion on broken faces. The local chain relations persist because their endpoints are perfect. The auxiliary families proving normalization are completed relative to the already chosen faces. They do not occur in the scalar expressions and do not require this action bound. □

7.5 Simultaneous geometric realization

Theorem 7.8 (Simultaneous geometric data)**.** *Use the actual local and terminal models of Proposition 3.1, the local fillings and framed arcs of Section 4, and the product Hopf-core bundle and correlated torus boundary of Section 4.3. Choose the all-L families of metrics and their local sphere and $S^{2,1}$ models before the equation perturbations, as above. Then for every $\delta > 0$ the finite system of operations in the three scalar expressions admits shared choices with the following properties.*

1. *The local and terminal complexes are the asserted actual perfect models, with good ordinary endpoint perturbations. Every occurrence of a labelled marked end uses the same complex and perturbation.*

2. *The composition, spectator-naturality and inverse-excision families have regular zero- and one-dimensional cut-down moduli spaces, with common data on their faces. Their compactifications give precisely the identities* (4.1), (4.3) *and* (4.9)–(4.12)*, with the common matching term $Q_{\mathfrak{a}}$. Ordinary Floer breakings are included, and tetrahedral bubble ends have even multiplicity over $\mathbb{F}_2$.*

3. *Every complete capped constituent of a scalar expression, including its ordinary source, cap and cobordism factors, has controlled data with $\eta + \epsilon/(32\pi^2) < \delta$. The bound is uniform through its stretched and broken faces.*

4. *The selected geometric all-L operation extends to the normalization construction with its counted boundary data fixed. The auxiliary normalization families that do not occur in those expressions are not required to satisfy this action bound.*

Proof. Choose the common endpoint data after the collared families of metrics. For the local and terminal ends, Proposition 3.1 supplies arbitrarily small perfect models. The additional good endpoint perturbations may vanish near the nondegenerate critical set, by [KM1, Section 3.2], so those generators are retained.

The explicit core and restriction calculations in Section 4.3 fix the partial marking, bundle sector and finite quotient. The local filling transitions and their framed arcs remain in product spectator regions. The product Hopf-tube markings on the ordinary factors are proper at the relevant ends. Thus the geometric composition and translation families have exactly the stated marked limiting pieces. This uses the underlying constructions, rather than assuming the analytic family statement of Proposition 4.2.

Every ordinary component and every torus-cut exterior component retains an ordinary strong end. The additional marking quotients restrict trivially there. Choose all nonlocal secondaries on product collars, leaving the complementary cores unperturbed. Proposition 7.3 gives universal surjectivity in these permitted spaces, including the relative parameter interiors. The finite quotient loses neither collar directions nor the four local tetrahedral branches at an ideal background.

For ordinary separating compositions and spectator translations, use the ordinary marked family compactification with the proper factors just described. For the torus faces, Proposition 7.6 gives the flat gluing charts and excludes additional torus-only pieces. Lemma 4.1 identifies the two surviving terms once each as $Q_{\mathfrak{a}}$. Their sum with ordinary composition and continuation gives the geometric inverse homotopy. These are statements about actual regular parameter ends; no homology excision isomorphism is being substituted for them.

Now follow the finite order of choices above. Boundary values agree because the same labelled factors and the same cut exterior were chosen first. Pull those values over parameter collars and extend relatively. Sard–Smale in the small open balls gives interior regularity; the ordinary and torus gluing charts give regularity near already fixed faces. Extend the dot sections compatibly and make them transverse separately. Proposition 7.7 and (7.11) give the prescribed bound on every capped constituent and its broken limits. In the perfect local complexes, the relative homology relations are literal chain relations throughout these choices.

For normalization, the complete local sphere and $S^{2,1}$ models, including their permitted generic metric family and corner data, were fixed before choosing the secondary perturbations in the families that define the counted J operations. These perturbations lie on external ordinary collars, outside the local pieces. Their sphere endpoints consequently agree with the fixed local corner models. The two ordinary-composition faces agree at their common corner because they use the same ordinary map data. The sphere-face exterior data extend between those corners; the isolated sphere model remains the published one. The special face likewise retains its preselected local model, and only its exterior perturbations require relative extension. The ordinary collar argument supplies that extension and the pentagon interior regularity. This completes the construction of [KM2, Sections 6–7] and its identity comparison with the counted faces fixed. Those additional families need not satisfy the smallness condition imposed on the scalar expressions. All four assertions follow. □

The theorem concerns realization of the specified operations. Scalar vanishing is obtained below by applying the uniform action estimate to their separately computed capped indices.

7.6 The action required by the index formula

We finish by applying the estimate to the scalar expressions. A term in one of these expressions counts configurations on several cobordism pieces, with matching critical points on their common

ends. Gluing their bundle data determines a closed bundle class. Its action is the sum of the actions on the pieces, even though a connection obtained by splicing the solutions need not itself be anti-self-dual. This allows us to combine the bound just proved with the closed index calculation in Section 6.

For a closed bifold (X, Σ) write

$$I_{\mathrm{top}}(X,\Sigma) = -\frac{3}{2}\big(\chi(X)+\sigma(X)\big) + \chi(\Sigma) + \frac{\nu(\Sigma)}{2} - \frac{\tau(\Sigma)}{2}. \tag{7.12}$$

Here $\nu(\Sigma) = \Sigma \cdot \Sigma$ is the self-intersection of [KM1, Definition 2.5], namely half the relative Euler number of the squared normal bundle with its canonical boundary section; τ is the number of tetrahedral points. The uncut deformation index is $8\kappa + I_{\mathrm{top}}$ by [KM1, Proposition 2.6]. This formula is additive over disconnected components. In particular one must not replace its ambient term by $-3(1 - b_1 + b^+)$ while silently changing the number of components.

Suppose a matrix-product term is represented by endpoint-matched solutions on its marked pieces. Use the matching isomorphisms to glue the bundle data. On a truncation, splice connections with a product collar at each matched end; exponential convergence lets the resulting action tend to the sum of the piece actions. This constructs a closed bundle class and gives additivity of Chern–Weil action. Fredholm index additivity across nondegenerate ends gives the corresponding index equation. The actual empty Hopf factor and acyclic torus flat factors have no continuous stabilizer or critical-manifold dimension to add to that equation. Their product closures have zero action and zero I_{top}. The matching-orbit identification of Lemma 4.1 preserves the exterior action and index; the two flat torus fillings add zero action.

The spliced connection need not solve the ASD equation. The action bound is applied to the original solutions on the pieces. Likewise, no equality between a closed point count and the algebraic trace is used. A trace-count identity would require the appropriate self-gluing class in the finite gauge subgroup; omitting it can change a covering multiplicity. It cannot change the local index or Chern–Weil integral of a given glued bundle class. Different bundle sectors may have different actions, but then the index equation assigns them different dimensions.

For the prescribed geometries, Proposition 6.4 gives

$$\chi(X) + \sigma(X) = 0, \qquad \chi(\Sigma) + \nu(\Sigma)/2 - \tau(\Sigma)/2 = 5/2.$$

Every constituent has one metric-family parameter. A dot imposes one real codimension, as in [KM1, Section 3.5]. Thus a zero-dimensional contribution with k dots must satisfy

$$0 = 8\kappa + \frac{5}{2} + 1 - k. \tag{7.13}$$

There is no additional parameter for each fixed ordinary factor in the product. The sole counted parameter belongs to the one homotopy factor.

Proposition 7.9 (Scalar vanishing)**.** *For the normalized scalar expressions of Proposition 5.2, with the capped geometries and dot counts of Proposition 6.4, one has*

$$\alpha = \beta = \chi = 0.$$

Proof. For three dots, (7.13) requires $\kappa = -1/16$; for two dots it requires $\kappa = -3/16$. Choose the data in Theorem 7.8 with $\eta + \epsilon/(32\pi^2) < 1/16$. Proposition 7.2 rules out every matched configuration that could contribute to any constituent. Hence each constituent count is zero and so are their finite sums. The cap summands for χ are used inside the fixed full expression; the argument does not require each summand to define an independent functional on the quotient containing the secondary operation. □

The scalar conclusion uses the realization theorem, the identity-normalized formula and the capped topological calculation together. The analytic construction supplies the small regular representatives; the fixed index equation supplies the negative action that excludes their contributions.

8 Assembly of the proposed proof

Proposed proof of Theorem 1.1. Propositions 2.2 and 2.3 identify the finite diagram and the three scalar tests. The local models of Proposition 3.1, together with Theorem 7.8, supply the geometric complexes with zero differential and compatible data for the local chain homotopies of Proposition 4.3.

In the inverse-excision comparison, the two torus limits are identified by the matching-orbit bijection of Lemma 4.1 and the low-dimensional gluing theorem, Proposition 7.6. They both give $Q_{\mathfrak{a}}$, with multiplicity one. Summing the four comparison homotopies therefore gives the geometric inverse relation used by that construction. The nonmatching coefficient $Q_{\mathfrak{b}}$ is not asserted to vanish and is not selected by either flat filling.

Proposition 4.4 gives a common primitive for the two full source boundaries. Lemma 5.1 transports it to the augmented all-L construction. The normalization clause of Theorem 7.8 preserves the chosen local sphere and $S^{2,1}$ models and completes the counted operation with its boundary data fixed. Proposition 5.2 consequently identifies the resulting scalar expression with $\ell h([c])$ for each required source and cap.

Every constituent has the topology and dot count of Proposition 6.4. Choose the simultaneous data with total action error strictly less than $1/16$. Propositions 7.2 and 7.9 exclude all zero-dimensional contributions, including matched broken products. Thus the three scalar coefficients vanish, and (1.1) gives $\dim J^{\sharp}(D) = 64$. □

8.1 Dependencies and the scope of review

The proof has three distinct inputs beyond its formal assembly. The matrices obtained by evaluating closed foams supply the octahedral reduction. The actual local perfect complexes allow homology relations to become literal chain relations. The marked families, their normalization, and the absolute index calculation identify the scalar counts to which the action estimate applies. None of these roles is supplied by the numerical agreement of the final ranks.

The simultaneous-realization argument is now included as a proof, with its permitted perturbation space, finite marking quotients, torus strata and choice order specified. It should be checked together with the constructions to which it is applied. In particular, one should follow the product Hopf bundle through the diagonal quotient and the matching cap framings, then through the local chain homotopies and the fixed local models used to normalize the all-L triangle. The resulting four-dimensional constituents must be the same ones whose signed normal data and indices are computed in Section 6.

The local-model claims of Proposition 3.1 remain a separate substantive part of that review, especially the cubic model at the central cube orbit. The finite extension calculation has an independently written implementation; the entire geometric pairing evaluator has not been independently reimplemented. Appendix A records these limits.

The dimension-64 conclusion remains provisional pending expert examination of the complete construction. If a step of the proposed argument fails, the finite calculation still leaves both 60 and 64.

A Computational specification and reproducibility

The supporting bundle is part of the finite specification of this draft. Its contents are sufficient to run the checks without the earlier research archives. Python 3, NumPy and SymPy are required. The manuscript can be typeset independently with a standard LaTeX installation. The command

```
python3 reproduce.py
```

from the bundle root runs the checks and writes a report and transcripts under `verification/`. It does not attempt to verify any analytic claim in this manuscript.

A.1 The independently reconstructed finite calculation

The directory `support/finite/` contains the new program `check_finite.py`. Its inputs are exact binary arrays with explicit inclusion, projection and quotient-lift maps. It imports no module from the earlier implementation. In particular it neither solves in the stored 48-dimensional Hom basis nor restricts extension variables by the auxiliary degree labels. All $25 \cdot 37 = 925$ entries of h are variables.

The program constructs a presentation using eleven independent exterior edges, different from the earlier chosen generator set. The presentation has 102 relations: 55 commutators, 18 quadratic vertex relations, 18 cubic vertex relations, and eleven cube relations. It builds the extension and intertwining equations directly, eliminates the extension variables first, and projects the solution space to the h coordinates. The recorded exact results are

Quantity	Lower extension	Upper extension
Variables	7,548	12,900
Nonzero equations	60,154	110,274
Rank of complete system	6,928	11,868
Rank of constraints on h	922	922
Dimension of projected space	3	3

Both projected spaces equal $\iota \operatorname{Alt}_3(\mathbb{F}_2)\rho$. The program writes its newly computed bases to `independent_obstruction_bases.npz`, and checks the normal form against them after solving the systems. It also checks the module relations, induced subquotient maps, ranks of s, γ, the source classes and the functionals defined by reflected foams, and all eight ranks of the alternating matrix. A separate recursive coloring enumeration within this program gives Tait counts $60, 48, 36, 72$ for D, K_0, K_1, L_1.

The independence is precisely at the level of equation construction and elimination from the retained matrices. It is not an independent derivation of those matrices from gauge theory. The file `independent_finite_result.json` states that scope and records input hashes. Running the script is an exact finite calculation over $\mathbb{F}_2$, with no floating-point rank tests or random sampling.

A.2 Geometric matrix inputs

The retained evaluator in `support/movies/` constructs the closed pairing movies from their half-foam reductions. Its certificate records local tetrahedral cancellations, disk-facet peels and residual sphere evaluations, or the nonbipartite seam obstruction. The mathematical evaluation rule is explained in Section 2. Running

```
python3 verify_foam_geometry.py --dots
```

within that directory checks the three Gram matrices, the two capped-map matrices, and all stored edge operators against this evaluator. The aggregate script also runs `check_faces.py` to check the facial supports. These are retained implementations. The transcripts supplied here record the runs accompanying referee-draft version 1; the unchanged finite checks have not been rerun merely for this integration. They are not newly independent evaluators.

The 97 undotted movie templates supply many matrix entries by changing their dot decorations. Their inventory, reduction commands and basis order are supplied in the JSON files in this directory. Binary matrix inputs are stored in NumPy's `.npz` format; shape and basis conventions are described in the root `README.txt` and the manuscript. The raw file names containing the word `combinatorial` are retained to preserve provenance; that name does not assert a general comparison between two homology theories.

A.3 Local and global geometric bookkeeping

The directory `support/local_models/` contains exact checks of the cube axis equations, terminal-model equations, the doubled theta/prism boundaries, and the four terminal reduction routes. The doubled triangle is checked as a six-vertex, nine-edge prism; its tangent calculation has eighteen variables and rank fifteen. These checks support the explicit geometric proofs in Section 3. They do not prove elliptic reduction or small-perturbation compactness.

The directory `support/geometry/` contains the ordered source and cap movies, the spherical rotation data, a check of every propagated facial move, and the exact signed port rotation and crossing-depth calculation. The arguments placing the foams in a common three-manifold and constructing their normal sections remain the written proofs in Section 6.

Finally, `support/assembly/term_assembly_check.py` checks the expansion of the scalar formula, with the domain and codomain of each map, the differential of the primitive and its terminal residual, the source and cap data, the local boundary assigned to each relation, one-parameter and dot counts, and the rational action arithmetic. Its catalogue counts labelled occurrences, not distinct moduli spaces. The number of optional continuation homotopies is immaterial; the mathematical statement is that the finite expansion is complete and each constituent has the stated type and topological index.

A.4 What the files do not certify

The finite checks do not establish that every operation in the formulas is realized by a regular marked family of metrics, that its compactification has the asserted ends, or that all its auxiliary data can be chosen with the required uniform bound on the perturbation error. Those are exactly the geometric and analytic claims addressed by the written arguments in Sections 4 and 7. The supporting readiness notes record the scope of the earlier reconstructed sections. Their historical statements of open requirements are superseded, for this integrated proposed argument, by the proofs now included here. They are not additional hypotheses or additional proofs of the analytic statements.

References

References to section, theorem, proposition, equation and figure numbers in [KM1]–[KM5] use the arXiv versions linked below, rather than the journal versions.

[KM1] P. B. Kronheimer and T. S. Mrowka, *Tait colorings, and an instanton homology for webs and foams*, J. Eur. Math. Soc. **21** (2019), no. 1, 55–119. doi:10.4171/JEMS/831. https://arxiv.org/abs/1508.07205v1.

[KM2] P. B. Kronheimer and T. S. Mrowka, *Exact triangles for $SO(3)$ instanton homology of webs*, J. Topol. **9** (2016), no. 3, 774–796. doi:10.1112/jtopol/jtw010. https://arxiv.org/abs/1508.07207v1.

[KM3] P. B. Kronheimer and T. S. Mrowka, *A deformation of instanton homology for webs*, Geom. Topol. **23** (2019), no. 3, 1491–1547. doi:10.2140/gt.2019.23.1491. https://arxiv.org/abs/1710.05002v2.

[KM4] P. B. Kronheimer and T. S. Mrowka, *Khovanov homology is an unknot-detector*, Publ. Math. IHÉS **113** (2011), 97–208. doi:10.1007/s10240-010-0030-y. https://arxiv.org/abs/1005.4346v1.

[KM5] P. B. Kronheimer and T. S. Mrowka, *Knot homology groups from instantons*, J. Topol. **4** (2011), no. 4, 835–918. doi:10.1112/jtopol/jtr024. https://arxiv.org/abs/0806.1053v2.

[ISST] H. Imori, T. Sano, K. Sato and M. Taniguchi, *Cobordism maps in Khovanov homology and singular instanton homology I*, arXiv:2505.12095v2 (2026). https://arxiv.org/abs/2505.12095v2.